1999-03

An infrared model of R/V POINT SUR using EOPACE data

Tan, Chee Yong

Monterey, California ; Naval Postgraduate School

NAVAL POSTGRADUATE SCHOOL
Monterey, California

THESIS

AN INFRARED MODEL OF R/V POINT SUR USING EOPACE DATA

by

Tan CheeYong

March 1999

Thesis Advisor: Alfred W. Cooper

Approved for public release; distribution is unlimited.

REPORT DOCUMENTATION PAGE

Form Approved
OMB No. 0704-0188

1. AGENCY USE ONLY *(Leave blank)*	2. REPORT DATE	3. REPORT TYPE AND DATES COVERED
	March 1999	Master's Thesis

4. TITLE AND SUBTITLE
An Infrared Model of R/V Point Sur using EOPACE data

5. FUNDING NUMBERS

6. AUTHOR(S)
Tan Chee Yong

7. PERFORMING ORGANIZATION NAME(S) AND ADDRESS(ES)
Naval Postgraduate School
Monterey, CA 93943-5000

8. PERFORMING ORGANIZATION REPORT NUMBER

9. SPONSORING / MONITORING AGENCY NAME(S) AND ADDRESS(ES)

10. SPONSORING / MONITORING AGENCY REPORT NUMBER

11. SUPPLEMENTARY NOTES
The views expressed in this thesis are those of the author and do not reflect the official policy or position of the Department of Defense or the U.S. Government.

12a. DISTRIBUTION / AVAILABILITY STATEMENT
Approved for public release; distribution is unlimited.

12b. DISTRIBUTION CODE

13. ABSTRACT ***(maximum 200 words)***

Infrared polarization techniques to improve the target-background contrast are the subject of much study lately. Polarized infrared images of the research vessel, R/V POINT SUR were taken extensively during the Electro-Optical Propagation Assessment in Coastal Environment (EOPACE) operational period in Mar-Apr 1996 at Point Loma, San Diego. Contrast improvement analysis of these images requires an infrared model of the research vessel.

This thesis models the apparent infrared signature of the R/V POINT SUR using ship skin temperature records from the EOPACE measurements. Using a simple geometric model and adopting a pixel-by-pixel approach, the emitted radiation for each pixel surface is calculated from the Planck radiation law. Radiation reflected off the pixel surface is estimated using the polarized SeaRad atmospheric propagation code. The total radiance is compensated for atmospheric transmittance with the Navy Aerosol Model to arrive at the apparent radiance at the sensor. The apparent radiance is translated into apparent temperature for comparison with the recorded images to validate the accuracy of the model. There is moderate agreement between the model and recorded images with 45-50% of the pixels falling within 1.75K of the measured apparent temperatures.

14. SUBJECT TERMS	15. NUMBER OF PAGES
Infrared, polarization, R/V POINT SUR, EOPACE, SeaRad, Navy Aerosol Model	106
	16. PRICE CODE

17. SECURITY CLASSIFICATION OF REPORT	18. SECURITY CLASSIFICATION OF THIS PAGE	19. SECURITY CLASSIFI- CATION OF ABSTRACT	20. LIMITATION OF ABSTRACT
Unclassified	Unclassified	Unclassified	UL

NSN 7540-01-280-5500

Standard Form 298 (Rev. 2-89)
Prescribed by ANSI Std. 239-18

Approved for public release; distribution is unlimited

AN INFRARED MODEL OF R/V POINT SUR USING EOPACE DATA

Tan Chee Yong
Major, Republic of Singapore Navy
B.A., University of Cambridge, 1990

Submitted in partial fulfillment of the
requirements for the degree of

MASTER OF SCIENCE IN PHYSICS

from the

NAVAL POSTGRADUATE SCHOOL
March 1999

Author: 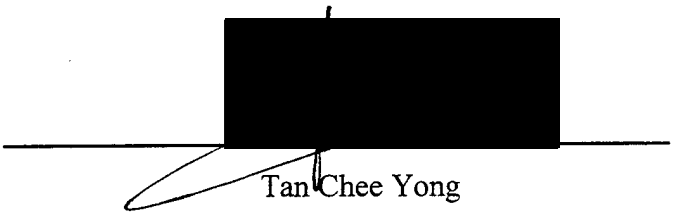
Tan Chee Yong

Approved by: 
Alfred W. Cooper, Thesis Advisor


Ronald J. Pieper, Second Reader

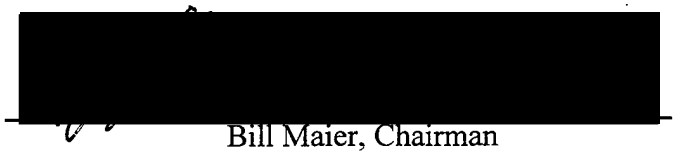
Bill Maier, Chairman
Department of Physics

ABSTRACT

Infrared polarization techniques to improve the target-background contrast are the subject of much study lately. Polarized infrared images of the research vessel, R/V POINT SUR were taken extensively during the Electro-Optical Propagation Assessment in Coastal Environment (EOPACE) operational period in Mar-Apr 1996 at Point Loma, San Diego. Contrast improvement analysis of these images requires an infrared model of the research vessel.

This thesis models the apparent infrared signature of the R/V POINT SUR using ship skin temperature records from the EOPACE measurements. Using a simple geometric model and adopting a pixel-by-pixel approach, the emitted radiation for each pixel surface is calculated from the Planck radiation law. Radiation reflected off the pixel surface is estimated using the polarized SeaRad atmospheric propagation code. The total radiance is compensated for atmospheric transmittance with the Navy Aerosol Model to arrive at the apparent radiance at the sensor. The apparent radiance is translated into apparent temperature for comparison with the recorded images to validate the accuracy of the model. There is moderate agreement between the model and recorded images with 45-50% of the pixels falling within 1.75K of the measured apparent temperatures.

TABLE OF CONTENTS

ACKNOWLEDGEMENT

The data analyzed in this research were obtained in part with funding support from NCCOSC-RDT&E under JO#MPE35R6SO1 Research Project RO3571. Support for the analysis was also received from the NPS Institute for Joint Warfare Research under the project Atmospheric EM/EO Assessments and Models.

I would like to express my appreciation to the people who made the EOPACE measurements. Specifically, I would like to thank the staff of the NPS Boundary Layer Group, the NPS Infrared Technology Group and the NCCOSC-NRaD for providing all the needed EOPACE data. I would also like to thank Professor Alfred W. Cooper for his guidance in the course of this thesis and Professor Ronald. J.Pieper for so readily agreeing to be the second reader despite the short notice. Lastly, I would like to thank my wife Elaine for her patience, support and understanding for the course of my studies at NPS.

I. INTRODUCTION

Every object is a source of infrared radiation with no exception even to the atmosphere through which the radiation propagates. Therefore, the design of infrared detection and tracking systems requires the ability to discriminate the object of interest from a highly cluttered environment. Various filtering techniques such as spectral and spatial filtering are typically used to achieve a detectable signal difference between the target and the background. More recently, polarization techniques to improve the target to background contrast in the infrared wavelengths are being seriously studied. Preliminary studies done at the Naval Postgraduate School using the Marine Aerosol Properties and Thermal Imager Performance (MAPTIP) trial data showed that the ship and the sky background exhibit no significant polarization features while the sea exhibits a considerable degree of vertical polarization at near grazing angles. [Ref.1 and Ref.2] The studies also showed that horizontal polarization filtering gives a 10 to 20% improvement for ship/sea contrast and up to 15% improvement for sea/sky contrast at the horizon. The analysis, however, was based on apparent radiance, that is, radiance measured at the sensor. It does not show how the relative contribution to the degree of polarization from the various sources and atmosphere add up to give the observed polarization features. A more conclusive study would need to account for the polarization features based on actual radiance derived from radiation theory. Such a study requires good environmental data and a reliable infrared model of the ship.

Electro-optical Propagation Assessment in Coastal Environment (EOPACE) organized by NCCOSC-NRaD (now, SpaWarSysCen.San Diego) is a 5-year multi-national effort to improve the performance assessment for electro-optical systems operating in a coastal environment. This is because the coastal environment may differ significantly from open ocean conditions, and existing propagation codes such as LOWTRAN/MODTRAN may not adequately account for the variations. While the main effort of the EOPACE measurement series is to fully characterize the coastal

environment, it also provided the opportunity to study the performance of polarization techniques. During one of the EOPACE operational periods in Mar-April 1996 at Point Loma, San Diego, extensive polarized infrared images of the research vessel, R/V POINT SUR were taken. With the comprehensive environmental database gathered during that period, it is possible to perform actual radiance calculations for the ship and the marine background.

This thesis models the apparent infrared signature of the research vessel R/V POINT SUR using ship skin temperature records from the EOPACE measurements. The research vessel is represented by a geometric model consisting of 23 vertical planes. Each plane is associated with a temperature reading from one of the 14 thermistors located around the R/V POINT SUR during the imaging period. To facilitate subsequent comparison with the recorded images, each plane is broken into pixel size surfaces. For each pixel size surface, the emitted radiation from the surface is calculated from the Planck radiation law. The radiation reflected off the pixel surface into the sensor is estimated from the environmental data using SeaRad [Ref.3]. SeaRad is a background add-on to the LOWTRAN 7 /MODTRAN atmospheric codes that calculates the sea radiance based on a Cox and Munk [Ref.4] wind driven capillary wave slope distribution. In the polarized SeaRad version, the total sea radiance is broken down into its vertically and horizontally polarized components. This feature allows us to derive the apparent radiance separately for the horizontal and vertical polarizations. For atmospheric compensation, the Navy Aerosol Model (NAM) developed specially for marine boundary layer propagation is used. Finally, the model is reconstructed into a 2-dimensional array with the elements giving the apparent radiance values for each pixel. The array is then compared with the ship pixels of the image arrays for each polarization to validate its accuracy. A reliable infrared model of the research vessel will offer many more options for future analysis, such as contrast improvement analysis, range improvement analysis and sensitivity analysis.

II. MODELING APPROACH

A. SURFACE RADIOSITY EQUATION

Modeling the infrared signature of a target or background is a complex process because every object is a source of both emission and reflection radiation. Hence, all infrared models are concerned with attempting to solve the surface radiosity equation [Ref. 5] :

$$L_s(\theta_r,\phi_r;\lambda)=\varepsilon_s(\theta_r,\phi_r;\lambda)B_s(T_s;\lambda)+\int f_i(\theta_i,\phi_i;\theta_r,\phi_r;\lambda)L_i(\theta_i,\phi_i;\lambda)d\Omega_i \qquad \textbf{(2.1)}$$

where L_s = spectral radiance of the surface S,

θ_r = zenith angle of the reflected radiation towards the sensor,

ϕ_r = azimuth angle of the reflected radiation towards the sensor,

θ_i = zenith angle of the incident radiation,

ϕ_i = azimuth angle of incident radiation,

λ = wavelength of the radiation,

ε_s = emissivity of the surface,

B = Planck 's function,

T_s = surface temperature,

f_i = Bi-directional Reflectance Distribution Function (BRDF) of the surface,

L_i = incident spectral radiance, and

Ω_i = incident projected solid angle

This equation essentially states that the spectral radiance of a surface element, S, is the sum of two components; the emitted radiation and the reflected radiation. The emitted radiation is the product of the Planck function at the temperature of the surface and the directional spectral emissivity of the surface. The reflected radiation is the integral over all the incident directions of the product of the incident spectral radiance for

an elemental projected solid angle of the source and the surface's BRDF.

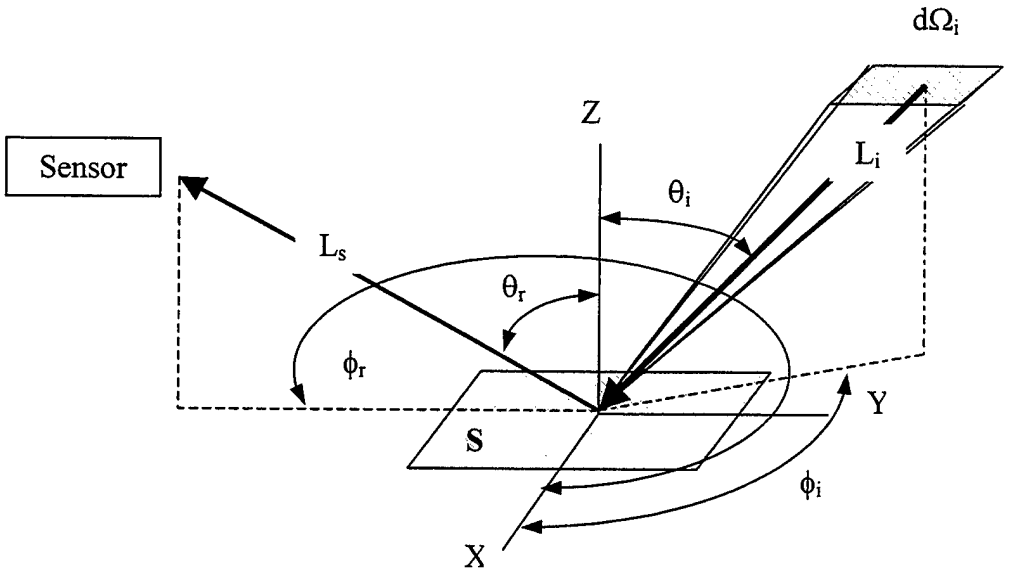

Figure 2.1. Diagram of geometric relationships [from Ref. 5]

The surface radiosity equation may seem to be a relatively simple equation to solve. However, this is not the case. For instance, there are inter-body reflections. Inter-body reflections involve radiation that is reflected to and fro between two surfaces. Hence, part of the incident radiance onto a surface may be radiance from the surface itself reflected off a second surface back to itself, and that portion of the incident radiance in unknown. Furthermore, performing the integral for reflected radiance is not easy and usually requires numerical methods. Given the limited time and resources available for this thesis, a more practical approach is to simplify the equation to a more useable form with a few assumptions.

Firstly, we see that inter-body reflections are at least twice reflected. In most cases, the reflectivity is low and hence, inter-body reflections can be reasonably neglected. Secondly, by assuming that the surface is perfectly diffuse, we can use the Lambertian approximation to eliminate the angular dependence of the emissivity and

reflectivity. Thirdly, assuming that the object behaves like a graybody, and making use of Kirchoff's law, we eliminate spectral dependence of the emissivity and reflectivity.

Hence, we obtain a simpler equation :

$$L_s(\lambda) = \varepsilon_s B_s(T_s;\lambda) + (1-\varepsilon_s)\int L_i(\theta_i,\phi_i;\lambda)\ \frac{d\Omega_i}{2\pi} \qquad (2.2)$$

We are still left with the task of performing the integral for reflected radiance, which is an angular average of the incident environmental radiance . For each surface element orientation, this integral average will be different and will have to be taken into account for a collection of elemental surfaces that may represent an object. A further simplification is needed and this will be discussed in the later section of this chapter.

1. Geometric Representation

To apply the surface radiosity equation to the problem , three basic issues would have to be settled first. The first issue is the geometric representation of the object of interest. The object of interest is the 135-feet research vessel, R/V POINT SUR, owned by the National Science Foundation and operated by the Central California Oceanographic Cooperative at Moss Landing Marine Laboratories, Monterey. During the recording period, it was used as the cooperative target for infrared imaging. The general data of the ship is given in Appendix A.

The simplest and most convenient way to represent any object is to use a collection of flat facets wherever possible. In fact, it is true to say that this is done in many infrared models. As observed from the infrared images of the ship at ranges of about one kilometer and more, intricate details of the ship are not readily apparent. Furthermore, given the relatively small look down angle at the sensor, all horizontal planes have a small viewable area, and do not contribute significantly to the emitted radiance. However, it should be noted that at grazing angles, radiance reflected off

horizontal planes may be significant. Nevertheless, we will neglect all horizontal planes and construct a simple scaled model of the ship using a collection of vertical planes. The geometric model is shown in Figure 2.2a and 2.2b below. The mast structure of the ship is not included as it is barely visible in most of the thermal images in this study. As mentioned above, the details at the bridge and 01 deck do not show up in the thermal images and they are modeled as simple cuboids here. The bow section is approximated as 2 regular vertical planes (planes 22 and 23). This makes the geometry analysis for the bow section much simpler. There are a total of 23 vertical planes, numbered as shown in the figures. The dimensions of each plane are given in Appendix A as well.

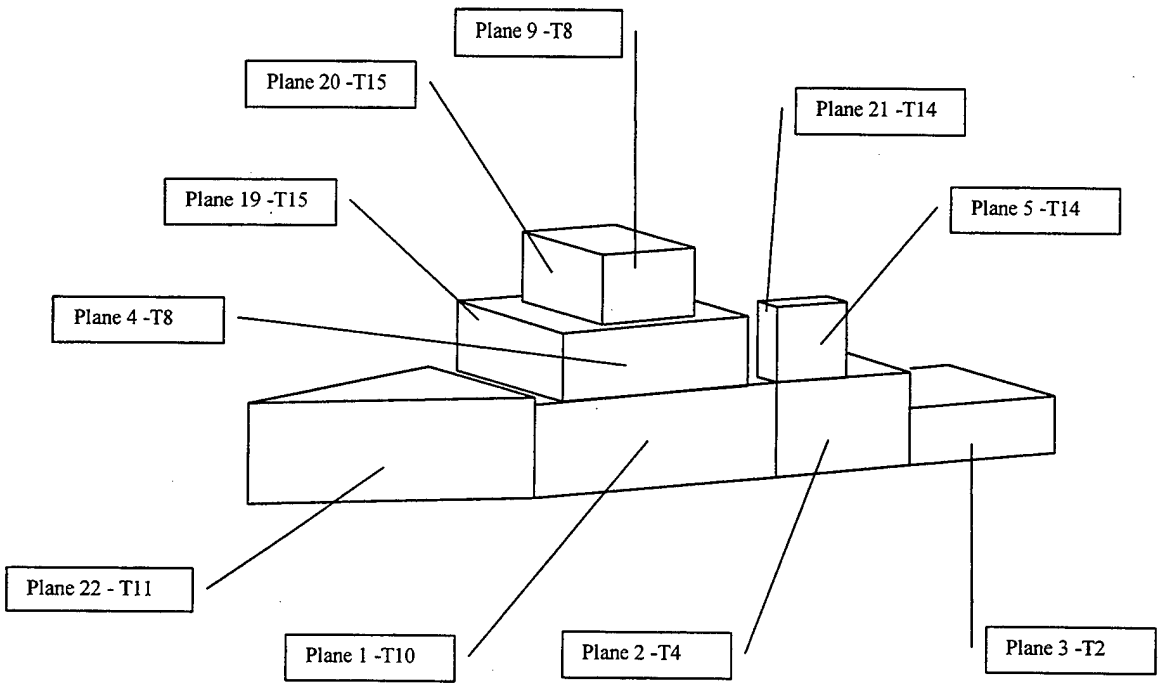

Figure 2.2a. Port view of the geometric model. and the plane-thermistor matching of R/V POINT SUR. The index number such as "T11" refers to the thermistor number as listed in Appendix B.

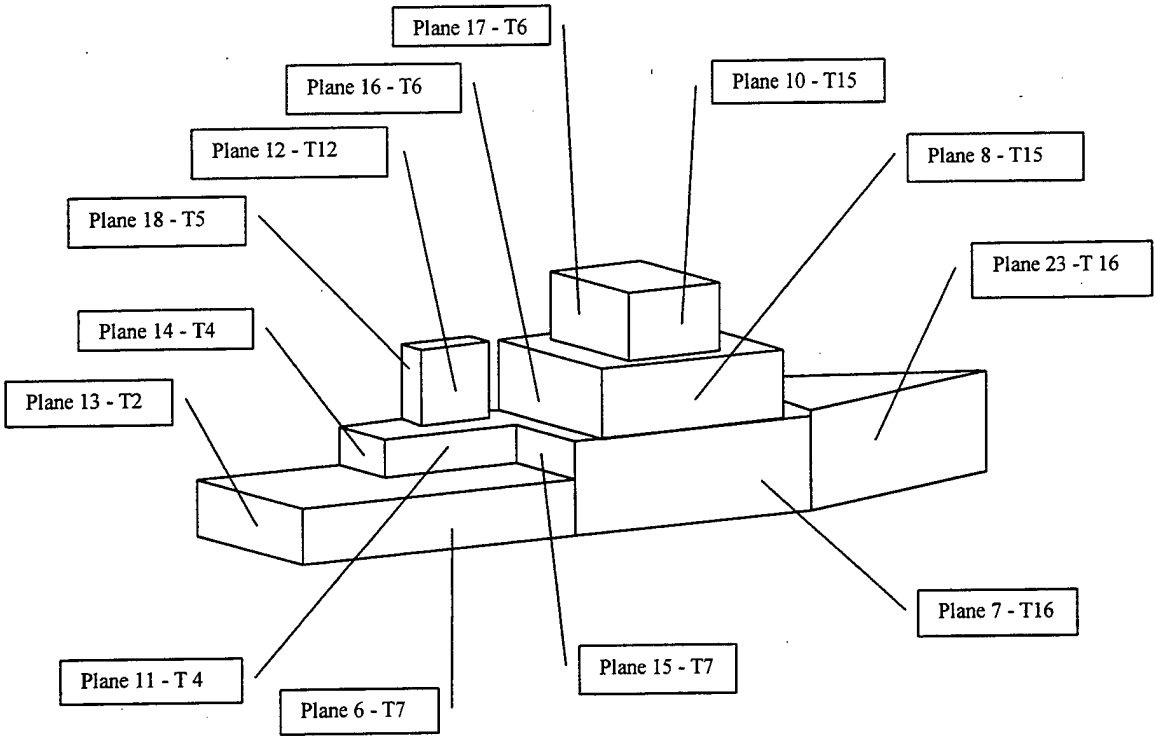

Figure 2.2b. Starboard view of the geometric model and the plane-thermistor matching of R/V POINT SUR

2. Surface Temperature

The second issue is to decide how these planes obtain their temperatures. This will allow us to calculate the emission term in the surface radiosity equation. One would have to consider the sources of heat generation on the ship, such as engines, running machineries, electrical switchboards, etc., the various heat transfer processes and also interaction with the environment to arrive at a "first principles" temperature distribution for the ship surfaces. This is by no means a simple task and is done in more advanced models such as Target Contrast Model 2 (TCM2) [Ref.6] adapted for use in the EOTDA FLIR Tactical Decision Aid Program. For our purposes, we require a simpler model.

For the period of the EOPACE imaging measurements, 14 thermistors were attached at selected locations around the R/V POINT SUR. The exact locations of the thermistors are listed in Appendix B. The thermistor readings were recorded at 20-second intervals throughout the whole imaging period. Hence, we can associate each plane of our geometric model with a temperature from one of the 14 thermistor readings.

In associating the planes to the temperature reading of a thermistor, it is also helpful to compare the apparent temperature distribution from the thermal images to the thermistor readings. Figure 2.3 below shows a sample thermal image. It can be seen from the image that there is a hot section that extends from the stack down to the hull on the port side of the ship. As a result, an additional plane was inserted (plane 2) to better reflect the temperature distribution of the hull on the port side. (See figure 2.2a) The matching of each plane to the temperature reading of a thermistor is indicated beside the plane number in Figure 2.2a and 2.2b above.

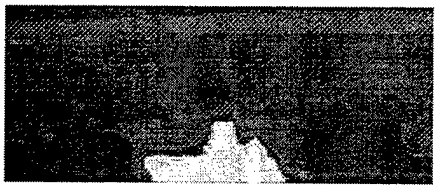

Figure 2.3 A typical portside view thermal image from file "Base01.pte". A hot section extending from the stack down to the hull of the ship is visible

3. Radiation from the Environment

There are two contributors to the reflected radiation term in the surface radiosity equation. Since we have ignored inter-body reflections, the environment is the sole source of reflected radiation.

Modeling of the environment is yet in itself another complex process. SeaRad with the Navy Aerosol Model is particularly suited for this case since it calculates sea radiance, reflected sky radiance, solar radiance, atmospheric path radiance, scattering and transmittance over the marine boundary layer atmosphere. However, like LOWTRAN 7 and MODTRAN, each input case is restricted to a point to point calculation. What this means is that the solid angle subtended by the source area has to be reasonably small for that calculation to be valid. Therefore, the correct approach is to consider the reflection off an elemental surface for each plane. To facilitate the subsequent comparison with the recorded images, the size of each elemental surface is made to coincide with the pixel size of the image.

Going back to our simplified equation 2.2, we are still left with the task of performing the integral for reflected radiance over the hemisphere of the elemental surface exposed to the environment. For each elemental surface, this integral would require approximately 50,000 input cases to SeaRad. Given the dimensions of R/V POINT SUR and the imaging ranges, it is estimated that each frame will have an average of 250 ship pixels. Thus, a huge amount of computational resources is needed for proper modeling. A further simplification is required here.

Consider a pixel surface, which is at a height, h, above the sea level. The range to the horizon for the given height h of the pixel is $\sqrt{(Rh)}$ where R is the radius of the earth. The angle of elevation of the horizon at the pixel is then given by $\tan^{-1}\sqrt{(R/h)}$. (See figure 2.4 below) Since h is very small compared to R, the value of $\sqrt{(R/h)}$ is very large. This gives α to be nearly 90 degrees. Therefore, each pixel will see the sky and sea as approximately two equal half hemispheres each subtending a solid angle of π steradians. If we assume that the incident sea and sky radiance are constant for their respective half hemispheres, then equation 2.2 becomes :

$$L_s(\lambda) = \varepsilon_s B_s(T_s;\lambda) + (1-\varepsilon_s)\left(\frac{L_{sea}}{2} + \frac{L_{sky}}{2}\right) \qquad \textbf{(2.3)}$$

where L_{sea} is the average sea radiance over the lower half hemisphere and

L_{sky} is the average sky radiance over the upper half hemisphere.

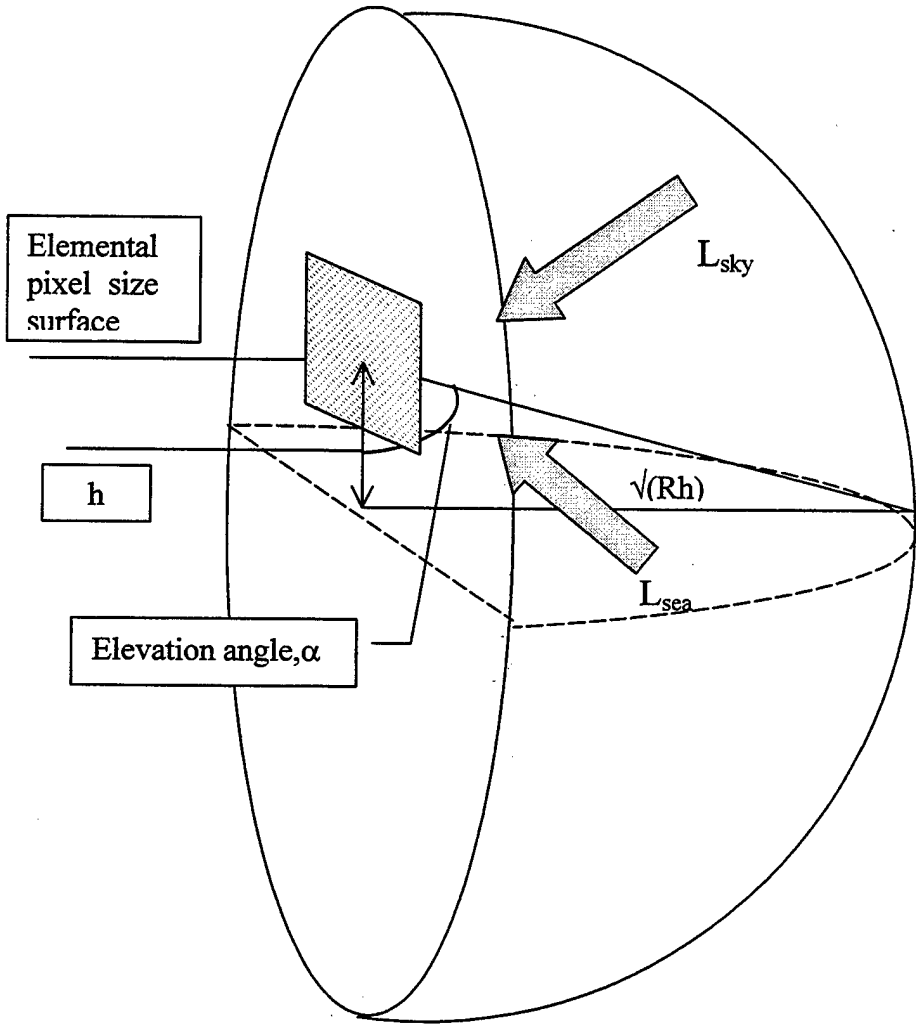

Figure 2.4 Geometry relation of a pixel with the sky and sea. Each pixel will see the horizon at nearly 90 degrees and hence, the sea and sky as two rougly equal half hemispheres.

For a cloudless sky, the sky radiance may be considered to be the sum of the sky background emission and the path radiance. It is reasonable to assume that the sky background is isotropic. Therefore, sky background emission is independent of look angle. However, the path length and hence, the atmospheric path radiance would increase

with increasing zenith angle towards the horizon. Hence, the most appropriate path to be used for SeaRad calculation so as to obtain the average sky radiance should be the path that gives the average path radiance. This was found to be the slant path to space at a zenith angle of 65.3 degrees.

For the average sea radiance, we will assume the sea to be a flat calm surface. The sea radiance is once again given by the surface radiosity equation 2.1. We can write the simplified equation as :

$$L_{sea} = B_{sea} - r(\alpha)(B_{sea} - L_{sky}) \qquad \textbf{(2.4)}$$

where r is the reflectance given by the Fresnel equations ,

α is the angle of incidence or elevation and

we have assumed here that L_{sky} is the average sky radiance.

We can see that L_{sea} is also a function of the zenith angle. Since B_{sea} and L_{sky} are both constant, the average L_{sea} is then given by the path for average reflectance. The path that would best represent the average sea radiance was found to be the slant path to the sea at a zenith angle of 118.1 degree. The details of both approximations are given in Appendix C.

III. IMPLEMENTATION

The modeling and analysis programs for this thesis were written in Interactive Data Language (IDL). However, SeaRad is a FORTRAN code written to run in an MS-DOS environment. Therefore, the implementation stage has to be divided into 3 parts, switching from IDL to MS-DOS and then back to the IDL environment.

In the first part, the programs perform 3 main functions. These are :

- to extract the relevant meteorological data required for SeaRad,
- to calculate the path geometry between each pixel and the sensor, and
- to write the meteorological and geometry data into the required input format for SeaRad.

For the second part, the main task is to run the input files through the SeaRad code. After running SeaRad, the tasks of the third part are :

- to extract the required data from the SeaRad output files
- to calculate the actual radiance received at the sensor
- to build a 2 dimensional array of the model that will facilitate subsequent comparison and analysis.

A list of the programs written for each part is given in Appendix D. The details of operations and information for each part are discussed in the following sections.

A. PART 1 - EXTRACT METEOROLOGICAL DATA, CALCULATE PATH GEOMETRY AND WRITE SEARAD INPUT FILES

There are 4 main procedures written for this part and they run in the sequence :

START.PRO, PLANEIN.PRO, SEAIN.PRO, AVESEAIN.PRO. Each main procedure performs a specific function. START.PRO extracts the relevant meteorological data. It also provides the basic geometry parameters to the procedure PLANEIN.PRO, which calculates the pixel coordinates and pixel-sensor path geometry. After all the required data are extracted and calculated, the procedures SEAIN.PRO and AVESEAIN.PRO are used to write the data into FORTRAN input format required to run the SeaRad code. The details given in the subsections below will more or less follow this sequence of operation.

1. Data File Format

The original infrared images of the R/V POINT SUR were recorded using the PTRWIN, version 3.16 data acquisition software from CEDIP. They are identified with the file extension .PTW. Although PTRWIN has the capability to analyze the images, it is inadequate for analysis with large numbers of images. Therefore, they were converted into a more efficient format using an IDL procedure written by Pontes [Ref. 7] called BASEGEN.PRO. The converted files, identified by the filename "BASE*.PTE", have a basic structure that contains an information vector, a time vector that gives the time of each frame and is followed by the images in the corresponding order. The detailed structure and type of information carried by each "BASE*.PTE" file is given in Appendix E.

Each "BASE*.PTE" carries a total of approximately 75 picture frames, that is, roughly 25 frames for each case of horizontally polarized, vertically polarized and unpolarized images. Given that the scanner produces 6.25 picture frames per second and that each image set of different polarization is taken sequentially, there is a time lag of about 8 seconds between the first frame and the last frame of the file. One of the objectives in the previous analysis performed by Pontes [Ref. 7] on the EOPACE data was to determine whether there is a ship radiance variation with time. It was found in that analysis that the variation of radiance within the time scale of 8 seconds is not significant. Therefore, only the first frame of each polarization case will be considered in this thesis.

2. Geometry of Measurements

The measurements were made from the NCCOSC Building 15 (32° 39' 55" N, 117° 14' 32" W, elevation above sea level -57 feet) at the tip of Point Loma. The research vessel was imaged at different aspect angles at ranges from 0.5 km up to 5 km. The bearing of the ship was also made to vary from about 100 to 260 degrees from the observation point. A chart showing the location of the measurement is in Appendix F.

3. Meteorological Data

Meteorological data were collected at 2 separate meteorological towers (METOC 1 and METOC 2) onboard the R/V POINT SUR. The data from METOC 1 and METOC 2 were recorded in files identified by "EOP*.TXT" and "EOP30SEC.*" respectively, where * indicates the day of the year. Each file was started at 0:00 Greenwich Mean Time (GMT) of each GMT day and the data were recorded in 30-second intervals. For each 30-second interval, 23 parameters were recorded. These are the GMT time of the reading, relative wind speed and direction, ship speed and direction, true wind speed and direction, air temperature, relative humidity, pressure, sea surface temperature and the GPS position of the ship. The detailed format of the METOC files is included as Appendix G.

To extract the meteorological data, the time vector in the .PTE file is first read. This is then converted to GMT to open the correct files and to read the nearest line of data recorded for that time. Since not all the data are needed, the relevant data are extracted, averaged and used to calculate some additional required information. The program READMET.PRO does all these, and returns a vector containing the range of ship, sea temperature, air mass parameter, current wind speed, 24 hour wind speed, wind azimuth relative to observer azimuth, GMT day of the year, GMT and observer azimuth. This information for the analyzed files is documented in Appendix H.

The US Navy Aerosol Model (NAM) was developed to compute the aerosol extinction coefficients for visual and infrared wavelengths in the marine boundary layer. Since we are concerned with the propagation of infrared radiation from a ship in a coastal environment , it is particularly suited for application in this thesis. However, in order to use the Navy aerosol model, part of the information required is the "air mass parameter (AMP)", which is included in the MODTRAN propagation code as "ICSTL". This parameter is not recorded in the METOC files and cannot be derived from any of the parameters collected there.

The traditional way to determine the air mass parameter is to measure the gas concentration of the radioactive Radon-222 in the atmosphere. During the Intensive Operational Period (IOP) in Mar-April 1996, the Radon-222 gas concentration was measured at San Nicolas Island, Point Mugu and San Diego. This information is available to the EOPACE participants at the EOPACE website at http://sunspot.spawar.navy.mil:80 /543/eopace/sd_iop_ma96/nrad883/bdg323/radon/radonsd.txt". With these measurements, the air mass parameter is then simply given by the equation [Ref.9] :

$$P = INT\left[\frac{Rn}{4}\right] + 1 \qquad \textbf{(3.1)}$$

where INT truncates to the integer value and Rn is the atmospheric Radon-222 gas concentration in picocurries per cm^3. It should be noted here that this equation is empirical and would have to be modified for application in other geographical regions. A brief discussion on the NAM and the air mass parameter is in Appendix I.

4. Pixel Size

The infrared scanner used to record the ship images is the dual band serial scanning AGA-780 Thermovision Thermal Imaging System. The short-wave (SW)

scanner uses an indium antimonide (InSb) detector and covers the 3-5.6 μm spectral band. The long-wave (LW) scanner covers the 8-14 μm spectral band and has a mercury-cadmium-telluride (HgCdTe) detector.

Electro-magnetic radiation from an object is focused onto the detectors by two separate systems of infrared lenses and rotating prisms. In each scanner, an infrared image frame is produced by 2 prisms, rotating in such a way that they produce four fields to make one interlaced frame. This is shown in Figure.3.1 below. Each field has 100 horizontal scanning lines and only 70 of these are used as active imaging lines. This gives a vertical scanning efficiency (η_{sc}) of 70%.

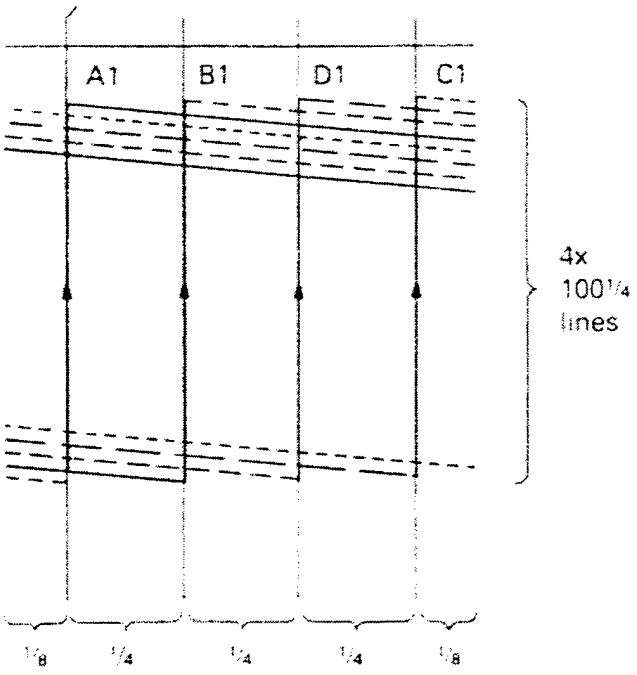

Figure 3.1 Interlace fields of the AGA-780 [Ref.9]

There were 3 different lenses that were available for use with the scanner. These are the 3.5°, 7° and 20° field of view (FOV) lenses. Table 3.1 lists the specifications for these lenses.

Table 3.1. Lens specification from AGA 780 Manual [Ref.9]

Lens	Min focus	Focal distance	Geometric resolution
3.5°	3.3m	191mm	0.5mrad
7°	1.0m	99mm	1.1mrad
20°	0.5m	33mm	3.4mrad

For the whole recording period during EOPACE April 96, only the 3.5° and 7° lenses were used. The horizontal pixel resolution is therefore 0.5mrad and 1.1 mrad respectively. To obtain the effective vertical pixel resolution, we multiply the geometric resolution by the scanning efficiency (η_{sc}) . This gives 0.35mrad and 0.77mrad for the 3.5° and 7° FOV respectively.

5. Path Geometry

The idea behind the path geometry calculation was to first determine the coordinates of the center of each pixel (which are called nodes) with respect to an origin vertically below the sensor. Thence, the sensor to pixel path is a vector given by the difference of the pixel coordinates and sensor coordinates.

To obtain the 3 dimensional coordinates of each node, we need to consider each plane of the geometric model of the ship (Figure 2.2, Chapter II) one at a time. The program PLANE.PRO is first used to select the visible planes for computation. This significantly reduces the computation load. Each selected plane is then broken down into nodes depending on the size of the elemental surface, which in turn, is a function of the range and pixel resolution. The position of each node relative to the center of the ship is first calculated. A rotation is then applied to the node positions to orientate the plane to the correct aspect angle. Lastly, the origin is shifted from the center of the ship to an origin directly below the sensor.

One of the main problems at this stage is the fractional edges of the planes. As each plane may not contain whole number of pixels, the edges have to be carefully handled so that when the neighboring plane is put together, it does not give an incorrect radiance value later on. To do this, the pixels at the edge are always rounded up. Then a weighting factor based on remaining area at the edge to the pixel area is calculated. For those pixels at the edge of a plane, the weighting would be less than one while the weighting for the pixels at the edge of the adjacent planes will be one minus the weighting of the edge pixels of the first plane. These pixels will share the same node positions. Therefore, the output of the routine PLANEIN.PRO contains a weighting matrix in addition to the 3 dimensional coordinates of the position of the nodes.

The reflection path was discussed towards the end of Chapter II. The paths representing the average sea and sky are just the slant paths with zenith angles of 118.1 and 65.3 degrees at the pixels respectively.

6. SeaRad [Ref. 3]

SeaRad was developed as an ocean background add-on to the MODTRAN 2 and LOWTRAN 7 atmospheric codes. The code used to calculate atmospheric transmittance, solar, sky and path radiance is the same code as MODTRAN/LOWTRAN. The sea radiance add-on is activated by a "seaswitch". When this switch is set to true, the code will take the boundary temperature as the sea surface temperature whenever the path intersects the sea surface. It then applies the Fresnel coefficients to the reflection of infrared radiation by a seawater capillary wave facet. The result of a single tilted facet is then integrated over all possible tilts which follows a Cox and Munk probability distribution function. Hence, SeaRad calculation gives a pixel average sea radiance, which suited our purpose here.

In addition, it is worth noting that SeaRad does not take into account the correction for shadowing effects proposed by Saunders [Ref. 10]. In essence, Saunders reasoned that radiation from certain portions of a wave is blocked by the wave in front.

Hence, these portions do not contribute to the sea radiance. The amount of area being blocked is dependent on the viewing angle. The more acute the viewing angle, the more area of the wave is blocked. Given the viewing geometry of our problem, this effect maybe appreciable.

SeaRad input requires the submission of a series of at least 5 cards. Each card is a line of formatted input. As each pixel requires one set of input cards and there is a large number of pixels, the routines SEAIN.PRO and AVESEAIN.PRO are used to write all the extracted meteorological data and calculated geometry data into the required format for each pixel. A sample input file is shown at Appendix J. An explanation of the input cards used for the input files is also included in Appendix J.

B. PART 2 - RUN SEARAD

SeaRad is run in an MS-DOS environment. The DOS commands to run a single input file are :

```
copy  "input filename"  tape 5
SeaRad
```

The output of the calculations is written to an output file called OUT. As can be seen, SeaRad is not designed to run a large number of input files as is needed here. Since each input file differs only in the geometry data, it would be possible to modify the SeaRad codes to accept multiple geometry inputs. A simpler alternative, though less efficient, is to run SeaRad in batches using MS-DOS batch file commands. A batch file called SEA1.BAT was written to run input files in batches. There are 3 types of input files in the "CASE1/INPUTS/" directory : the first type is for the pixel-sensor path geometry , the second type for the pixel-sea geometry and the last type for the pixel-sky geometry. These files are identified by the filename "*p*c**.std", "*a*b*0.std" and "*a*b*1.std" respectively. The output of each file has exactly the same name as the input file but they are copied into the "CASE1/OUTPUTS/" directory.

C. PART 3 - EXTRACT SEARAD OUTPUT, CALCULATE RECEIVED RADIANCE AND CONSTRUCT 2-D ARRAY

After running SeaRad, the procedure CONTINUE.PRO reads the SeaRad output files to extract the required information. It then calculates the radiance received at the sensor and reconstructs the model into a 2 dimensional array. The second section of CONTINUE.PRO compares the resultant array with the recorded image arrays. The second section will be discussed in the next chapter.

1. SeaRad Output

The format of the SeaRad output files depend on the type of calculation that is done. For the three input cases, two types of output files were written. A sample of each type of output file is shown in Appendix K. The routines SEAOUT.PRO and AVSEAOUT.PRO are used to extract the required information from the output files. The information returned by these programs is :

- pixel to sensor path transmittance (τ_{path}),
- pixel to sensor path radiance (L_{path}),
- total radiance at the pixel for the average sky radiance path (L_{sky})
- total radiance at the pixel for the average sea radiance path in horizontally polarized (L_{Hsea})., vertically polarized (L_{Vsea}).and randomly polarized components (L_{Usea}).

2. Ship Skin Temperature

As previously mentioned, the ship skin temperatures of R/V POINT SUR were recorded continuously in 20-second intervals throughout the whole measurement period. These readings were stored in a file called "SKINDATA.PTE". Each line has 16 readings corresponding to 2 reference temperature readings and 14 thermistor readings.

The detailed format for the skin temperature file is in Appendix L.

3. Ship Skin Radiance

Given the ship skin temperature, the spectral radiant exitance from the ship skin surface can be calculated using Planck radiation law :

$$M_{BB}(\lambda,T) = \frac{2\pi hc^2}{\lambda^5 (e^{hc/\lambda kT} - 1)} \tag{3.2}$$

where T is the surface temperature in K,

λ is the wavelength in m

h is Planck's constant (6.6256×10^{-34} Js),

c is the speed of light (3×10^8 m/s),

k is Boltzman's constant (1.38054×10^{-23} J/K) and

M_{BB} has dimensions in watts per meter square per wavelength interval in m.

The radiant exitance for a graybody over π steradians of solid angle is then given by the Stefan-Boltzman law, which is :

$$M_{Graybody}(T) = \varepsilon \int_0^\infty M_{BB}(\lambda,T)d\lambda = \varepsilon\sigma T^4 \tag{3.3}$$

where ε is the emissivity of the surface and

σ is the Stefan-Boltzman constant (5.6697×10^{-12} W/cm^{2}K^4).

However, we are only interested in the in-band radiance for the long-wave band (8-12 μm). The in-band radiance can be represented as :

$$L_{surface} = \frac{\varepsilon}{\pi} \int_{8\mu m}^{12\mu m} M_{BB}(\lambda,T)d\lambda \tag{3.4}$$

There are two methods to calculate the in-band radiance. One method is to use the universal blackbody curve or pre-tabulated integrals over it. The other method is to perform the integration numerically. The routine "EMISSION.PRO" performs the numerical integration using step size of 0.01μm.

Since we have already associated each plane with the temperature reading of a thermistor, the in-band radiance is calculated for each pixel using the above equation. In the calculations, the ship surface is assumed to behave like a graybody with an emissivity previously measured to be 0.95. Since no further information on the optical properties of the ship paint is available, another assumption was made that the horizontal and vertical polarized components of the in-band radiance are equal.

4. Radiance Received at Sensor

Finally, the radiance received at the sensor is the sum of the ship skin radiance compensated for atmospheric transmittance, the path radiance and the reflected sea and sky radiance. This is best summarized by the following formulae for the two polarized and randomly polarized components :

$$L_{Hsensor} = \frac{1}{2}\left[\tau_{path} L_{surface} + L_{path} + (1-\varepsilon)\tau_{path}\left(L_{Hsea} + \frac{L_{sky}}{2}\right)\right] \qquad \textbf{(3.5a)}$$

$$L_{Vsensor} = \frac{1}{2}\left[\tau_{path} L_{surface} + L_{path} + (1-\varepsilon)\tau_{path}\left(L_{Vsea} + \frac{L_{sky}}{2}\right)\right] \qquad \textbf{(3.5b)}$$

$$L_{Usensor} = \tau_{path} L_{surface} + L_{path} + \frac{(1-\varepsilon)}{2}\tau_{path}\left(L_{Usea} + L_{sky}\right) \qquad \textbf{(3.5c)}$$

It should be noted here that there would be a transmission loss due to the polarizing filters. However, it is not necessary to correct for it since the corrections are built into the scanner calibration process.

5. Reconstructing a 2-D Array

Remembering that the procedure was done one plane at a time, the remaining task is to put all the planes together to give a 2 dimensional image of the model. This process is done in 3 steps.

The first step is to multiply the radiance matrix of each plane by the weighting matrix so that the pixels at the edges of adjacent planes will fit together. The second step is to correctly position each plane relative to a reference point (the origin at the midpoint of the ship) in an empty 72 x 30 matrix. This is done by the procedure PLACE.PRO. An additional procedure called BLOCK.PRO is then applied to blank out the areas of overlap between planes for that viewing angle. Lastly, the radiance values of the planes are simply added together to form a 2D array of ship radiance received at the scanner. A sample image(magnified) of the ship model derived for file "Base01.pte" is shown in Figure 3.2 below. The recorded image is the original image from the data files. The extracted image is the resultant image when a mask having the same shape as the model but containing ones and zeros is applied to the original images.

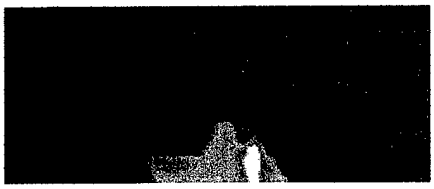

Recorded image

Model

Extracted image

Figure 3.2 Images of R/V POINT SUR for unpolarized case from file Base01.pte. The model image shows a higher temperature than the recorded temperature in the extracted image. Notice that some of the background pixels are inevitably included in the extracted image

IV. COMPARISON OF RESULTS

A. APPROACH FOR COMPARISON

1. Pixel-by-pixel Comparison

Since we started out using a pixel by pixel approach to derive a 2-dimensional array for received radiance at the sensor, each element in the 2-D array will directly correspond to a pixel in the recorded image frame. Each image frame has a sea and sky background. Since we are only interested in comparing the ship model with the measured ship radiance the background would have to be eliminated. To extract the ship pixels in the image frame, a mask is first created from the 70 by 30 model array. This is done by setting elements of ship pixels in the array to ones and the background to zeros. Next, the coordinates of the right bottom corner of the ship in the image frame are read from user's input. This information is used as the reference point for aligning the mask over the image frame to extract the ship pixels in the image. Having set all the background elements of the image array to zero, we can now compare the two arrays directly by simply taking their difference. However, before the difference can be taken, the elements in the arrays must have the same units. The model array has units of radiance while the image array has units of digital level. A unit conversion is required.

2. Thermal Level

The numerical measure of the received and detected radiation used in the infrared scanner is called the thermal level. The traditional unit for the thermal level is the isotherm unit, which is linearly related to the received photon radiation. Therefore, the relationship between the thermal level and the object temperature is non-linear. To translate object temperature to its thermal level, a calibration function is used. This calibration function is obtained by plotting the thermal level against the known

temperature of a blackbody. It has a characteristic equation of a form similar to the Planck equation :

$$TL = \frac{A}{Ce^{B/T} - 1} - OS \tag{4.1}$$

where A, B, C are constant determined by curve fitting,
OS is the offset correction for detector drift and
T is the temperature in K.

The calibration function is dependent on the aperture and filter used and a set of calibration curves is usually produced. Prior to the measurement period, the scanner with polarizing filters was calibrated. The calibration curves are shown in Appendix M. The calibration constants for each polarization filter are also given in the appendix. Although all the calibration constants are given, it should be noted here that the offset constant for detector drift, OS, tends to vary rapidly with changing ambient conditions. Using the calibration functions, the thermal level of the ship pixels for each polarization case in the images can be easily translated to the equivalent blackbody temperature of the ship surfaces.

3. Digital Level

It was found that the images recorded by the PTRWIN software were stored in digital levels in the original data files. Although the PTRWIN software have the function to convert digital levels to isothermal units, the process to convert all the "*.PTE" files into thermal levels would require re-storing the original "*.PTW" file into isothermal units and re-generating the "*.PTE" files using BASEGEN.PRO. An alternative way is to deduce the relationship between the digital level and thermal level from the PTRWIN software. It was found that they are related by a simple linear relation which depends on the Range (R) and Level (L) settings in the PTRWIN software. Hence, to convert digital level (DL) to thermal level (TL), the following empirical formula is used :

$$TL = A * DL + B \quad (4.2)$$

where $A = 0.00122$, $B = L - 2.5$ for $R = 5$,

$A = 0.00244$, $B = L - 5$ for $R = 10$ and

$A = 0.00488$, $B = L-10$ for $R = 20$.

The range and level settings are not available in the information vector of data (*.PTE) files. They have to be extracted from the original data (*.PTW) files. Appendix N documents the original files and their range/level settings.

3. Calibration Drifts

The time lag between the first frames of the horizontally and randomly polarized images in a single data file is roughly 8 seconds. Within this time scale, the temperature distribution of the ship surfaces has not changed significantly. If we translate the first image frame of each polarization in a data file into the equivalent blackbody temperature using the calibration curves, we should expect the blackbody temperature arrays for the three different polarizations to be almost similar, that is, a pixel in one polarization frame should have the same equivalent blackbody temperature as the corresponding pixel in another polarization frame. Hence, if we take the difference between the blackbody temperature arrays of any two polarizations, the elements of the resultant temperature difference matrix would be mostly zeros. In another way, the average value of all the elements in the resultant temperature difference matrix should be nearly zero. Table 4.1 below shows the average values of the elements of the resultant temperature difference matrices when the blackbody temperature arrays of the three different polarizations of a single data file are compared to each other. Column one gives the average temperature difference between horizontal and vertical polarizations; column two , horizontal and random polarizations; and column three vertical and random polarizations.

Table 4.1 Mean pixel temperature difference between polarization cases of an image file

Filename	Average temperature difference (K)		
	H-V	H-U	V-U
Base09.pte	-0.053289222	-6.0796106	-6.0263214
Base10.pte	-0.063456130	-4.8232400	-4.7597838
Base11.pte	0.094446067	-5.2094861	-5.3039322
Base15.pte	0.029233603	-4.7203123	-4.7495459
Base16.pte	0.23777563	-4.1678803	-4.4056560
Base28.pte	0.55287224	-1.4238610	-1.9767332
Base30.pte	0.21753705	-1.3070561	-1.5245932
Base32.pte	-0.45393654	-3.3308119	-2.8768753

We can see that the temperature differences between corresponding pixels of the polarized image and unpolarized image are significant. If this difference were solely due to the contrast improvement of the polarizing filters, we should expect opposite signs for the second and third columns. Clearly, this is not the case and it is likely that calibration drifts are present. Since we do not know exactly what the calibration drifts are, a relative calibration is required in order for us to relate the measured ship skin temperatures to the recorded thermal levels. The procedure for a relative measurement is described in section 10 of the AGA manual [Ref.10]. The relevant extract is reproduced in Appendix O.

To perform the relative calibration, we use the following formula from the AGA manual :

$$I_o = \frac{\Delta I_{or}}{\tau_o \varepsilon_o} + I_r \qquad (4.3)$$

where I_o is the relative calibrated thermal level,

I_r is the calibrated thermal level of a reference point on the object whose temperature is known,

ΔI_{or} is the thermal level difference from the reference level (I_r),

τ_o is the atmospheric transmittance between object and scanner and

ε_o is the object emissivity.

Since the values of the elements of the matrix that we derived are radiance values received at the scanner aperture, these would have to be converted into equivalent blackbody temperatures. The routine RADTOT.PRO converts radiance to equivalent blackbody temperature by linear interpolation in three iterations. Since the radiation-temperature relation is actually non-linear, a good initial guess of the temperature range is required to achieve good conversion accuracy. For the temperature range of the ship, the conversion accuracy is 0.001 W/m^2.

If we now use the converted blackbody temperature of the pixels for the recalibration, then τ_o and ε_o are simply equal to one in equation 4.3 since these are the equivalent blackbody temperatures at the aperture of the scanner. In addition, any pixel can be used as the reference point since now they each have a known equivalent blackbody temperature.

4. Unit of Comparison

The comparison can be done using radiance, temperature or thermal level differences. However, thermal level differences do not give a good indication when we

compare across polarization cases. For example, a thermal level difference of 1 in the horizontal polarization case may be due to 0.3 W/m^2 difference in radiance while a difference of 3 isotherm units in the unpolarized case is just 0.15 W/m^2. Hence, doing the comparison in temperature units is the most convenient since the recalibrated thermal levels of the image pixels are easily translated to temperature.

B. DISCUSSION ON RESULTS

1. Statistical Measures

In an ideal case, the temperature difference between each pixel of the model and the recorded image would be zero. More realistically speaking, we would expect a distribution of pixels with a mean of close to zero and a small standard deviation. Figure 4.1 below shows the pixel distributions for a sample file. From the figure, a large number of pixels are clustered close to the zero temperature difference mark. However, there are a small percentage of pixels that register a big temperature difference. The origins of these outlying pixels are likely due to two limitations.

The first limitation is inherent in the geometric representation of the ship. As our geometric model is a simplified representation of the ship, not all calculated pixels will have a corresponding pixel in the image or vice versa. Secondly, the alignment of the mask is highly sensitive, that is, down to pixel resolution. At this level of resolution, it is difficult to achieve a 'correct' one to one correspondence in the ship pixels. The impact of all this is that some pixels will be compared with the background pixels resulting in a big temperature difference. It has the effect of driving up the mean and standard deviation especially when the number of ship pixels is small.

In order to obtain a better characterization of the pixel distribution, two additional statistical measures were calculated. These are the modal temperature difference and the fraction of pixels falling within a specified range from the modal temperature difference.

The modal temperature difference has the advantage that it is not affected by the outlying pixels. However, it is more susceptible to freak occurrence of peaks in a distribution. Therefore, both sets of statistical measures are needed to gain a fair interpretation of the results.

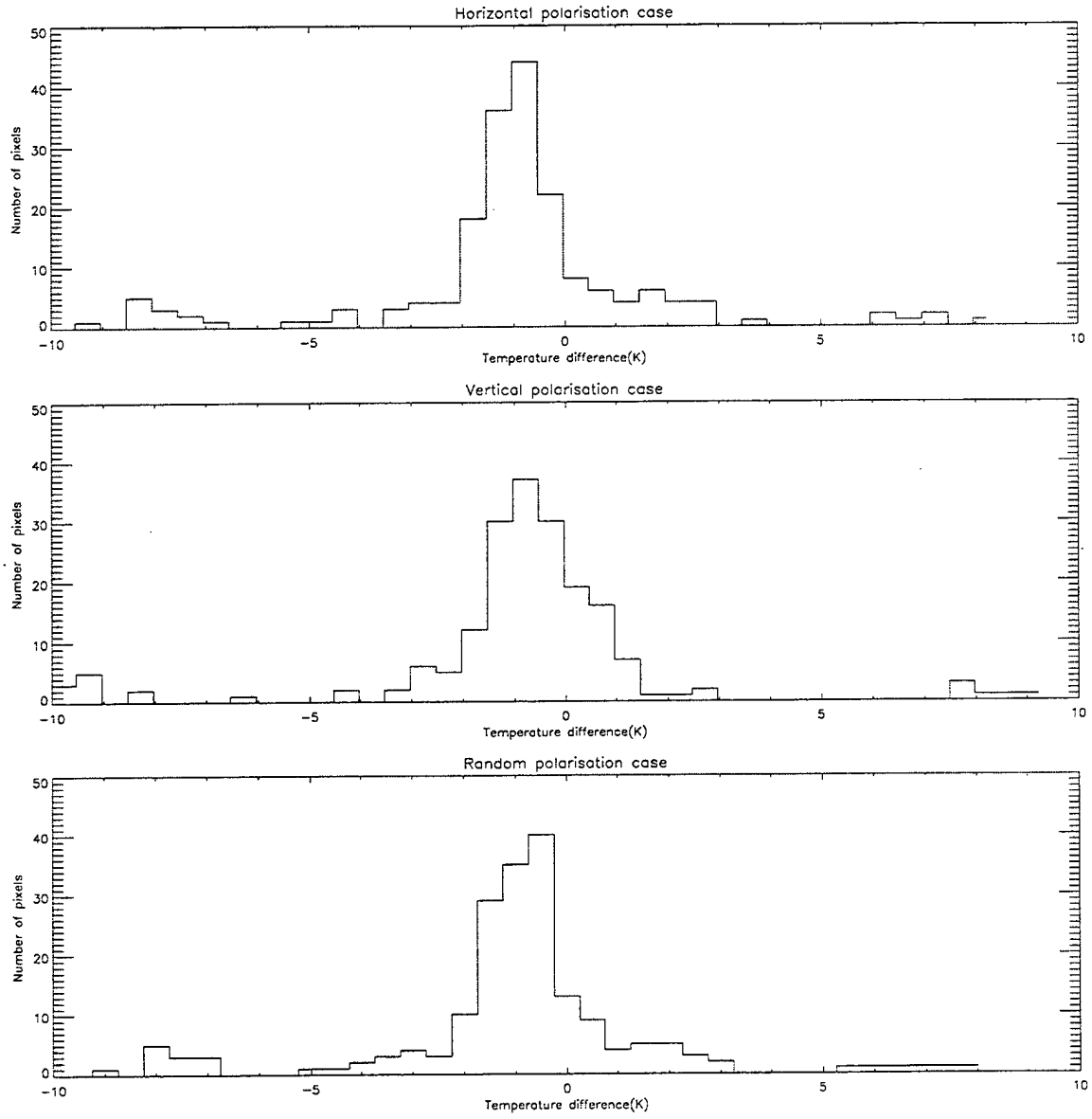

Figure 4.1 Pixel distribution of difference in equivalent blackbody temperature between model and recorded image for file Base10.pte. The small percentage of pixels at the outlying areas tend to drive up the mean and standard deviation

2. Results of Comparison

A total of 37 data files were analyzed and compared. The results of each comparison are tabulated in Table 4.2. Most of the cases analyzed showed a modal temperature difference of less than 1K between model and image. The average temperature differences for these cases were also less than 1K. The modal temperature difference, in general, is lower than the average temperature difference.

There are 5 files where the modal temperature difference is much higher than the average temperature difference. The modal temperature differences for the 3 polarization cases in these files were very different as well. In contrast, the average temperature differences for the 3 polarization cases were quite consistent. It is likely that there are occurrences of freak peaks in the distribution making the modal temperature difference unreliable.

There is one file that has average and modal temperature differences of more than 2K for all 3 polarization cases. This is file Base07.pte. The total number of pixels for each frame of this file is 32. It is likely that there are too few good pixels to give a reasonable comparison. With the exception of file Base07.pte, there is moderate agreement between the model and recorded images with 45-50% of the pixels falling within 1.75K of the measured apparent temperature.

Table 4.2 Comparison of temperature between model and recorded images

File no. (base*.pte)	Number of pixels	Polarisation case	Measure of centre of distribution		Measure of spread		
			Modal temperature difference	Mean temperature difference	Fraction of pixels within 0.25 K of modal temp. difference	Fraction of pixels within 0.75 K of modal temp. difference	Standard deviation
01	158	H	1.835	2.391	0.266	0.437	4.844
		V	1.182	1.223	0.222	0.459	4.488
		U	0.000	-0.282	0.367	0.602	3.033
02	160	H	1.566	1.332	0.219	0.506	4.780
		V	0.099	0.218	0.188	0.526	3.007
		U	-0.476	-0.569	0.288	0.553	2.026
03	82	H	-0.389	1.136	0.280	0.476	3.617
		V	0.169	1.448	0.293	0.488	3.578
		U	0.016	1.388	0.171	0.349	3.730
04	47	H	-2.726	0.212	0.128	0.213	4.894
		V	-0.274	0.136	0.213	0.434	3.552
		U	-0.787	-0.511	0.277	0.533	2.906

File no. (base*.pte)	Number of pixels	Polarisation case	Measure of centre of distribution		Measure of spread		
			Modal temperature difference	Mean temperature difference	Fraction of pixels within 0.25 K of modal temp. difference	Fraction of pixels within 0.75 K of modal temp. difference	Standard deviation
05	59	H	-0.926	0.630	0.153	0.356	3.489
		V	-0.325	-0.051	0.322	0.517	3.722
		U	-0.254	-0.372	0.169	0.467	3.430
06	59	H	-0.853	1.687	0.136	0.322	3.063
		V	-0.415	0.336	0.186	0.424	2.529
		U	-0.708	-0.589	0.237	0.475	2.703
07	32	H	-6.847	-3.320	0.125	0.188	3.729
		V	-5.800	-3.892	0.156	0.250	3.652
		U	-1.939	-3.118	0.125	0.219	3.941
08	93	H	-0.466	1.602	0.172	0.323	2.540
		V	0.385	0.117	0.237	0.441	2.266
		U	0.092	0.536	0.215	0.516	2.271
09	151	H	-0.360	-0.174	0.225	0.444	2.764
		V	-0.240	-0.154	0.179	0.450	2.862
		U	-0.359	-0.628	0.199	0.437	2.553

File no. (base*.pte)	Number of pixels	Polarisation case	Measure of centre of distribution		Measure of spread		
			Modal temperature difference	Mean temperature difference	Fraction of pixels within 0.25 K of modal temp. difference	Fraction of pixels within 0.75 K of modal temp. difference	Standard deviation
10	190	H	-0.794	-0.908	0.232	0.537	3.006
		V	-0.783	-0.775	0.195	0.511	3.130
		U	-0.495	-0.882	0.211	0.463	2.922
11	191	H	1.126	-1.121	0.079	0.194	4.676
		V	-0.371	-2.162	0.147	0.418	3.489
		U	-0.449	-1.092	0.200	0.445	3.484
12	45	H	1.421	-0.208	0.156	0.267	5.154
		V	-0.057	0.034	0.111	0.244	4.493
		U	0.569	-0.352	0.200	0.477	3.078
13	55	H	1.016	1.158	0.145	0.327	3.750
		V	-0.300	1.194	0.291	0.509	3.310
		U	0.487	1.528	0.200	0.491	3.429
14	80	H	-0.165	-0.854	0.200	0.475	3.423
		V	-0.471	-0.824	0.225	0.550	3.390
		U	-0.943	-0.772	0.200	0.425	3.360

File no. (base*.pte)	Number of pixels	Polarisation case	Measure of centre of distribution		Measure of spread		
			Modal temperature difference	Mean temperature difference	Fraction of pixels within 0.25 K of modal temp. difference	Fraction of pixels within 0.75 K of modal temp. difference	Standard deviation
15	92	H	-0.945	-0.209	0.207	0.511	1.917
		V	-0.164	-0.070	0.228	0.505	2.219
		U	-0.931	-0.932	0.228	0.467	1.793
16	98	H	-0.945	0.569	0.153	0.378	2.64
		V	-0.324	-0.328	0.173	0.388	2.443
		U	-1.713	-0.393	0.194	0.429	2.425
17	54	H	-0.482	1.369	0.204	0.444	4.865
		V	-0.274	1.425	0.352	0.444	4.850
		U	0.132	1.930	0.148	0.315	4.674
27	51	H	-0.362	-1.982	0.333	0.392	2.998
		V	-0.392	-1.823	0.275	0.392	2.938
		U	-1.697	-1.872	0.196	0.392	3.056
28	79	H	-0.246	3.617	0.165	0.241	5.072
		V	-0.183	0.388	0.317	0.615	3.256
		U	-0.181	0.292	0.354	0.582	3.554

File no. (base*.pte)	Number of pixels	Polarisation case	Measure of centre of distribution		Measure of spread		
			Modal temperature difference	Mean temperature difference	Fraction of pixels within 0.25 K of modal temp. difference	Fraction of pixels within 0.75 K of modal temp. difference	Standard deviation
29	105	H	-0.428	0.617	0.152	0.238	3.860
		V	-0.195	-0.698	0.286	0.600	3.674
		U	-0.441	-0.703	0.333	0.600	3.629
30	24	H	-0.258	0.990	0.375	0.417	3.630
		V	-0.011	0.891	0.250	0.542	3.751
		U	0.837	1.182	0.167	0.240	4.782
31	30	H	-0.631	2.565	0.367	0.667	6.220
		V	-0.016	2.736	0.400	0.667	6.260
		U	-0.240	1.239	0.167	0.355	6.269
32	33	H	0.043	1.489	0.212	0.364	5.878
		V	-1.275	1.632	0.152	0.182	5.672
		U	1.105	1.738	0.152	0.324	6.713
33	29	H	-0.110	-0.027	0.345	0.621	2.038
		V	0.794	0.500	0.379	0.552	2.124
		U	-2.600	-1.427	0.172	0.233	3.227

File no. (base*.pte)	Number of pixels	Polarisation case	Measure of centre of distribution		Measure of spread		
			Modal temperature difference	Mean temperature difference	Fraction of pixels within 0.25 K of modal temp. difference	Fraction of pixels within 0.75 K of modal temp. difference	Standard deviation
34	46	H	0.697	0.241	0.174	0.413	5.223
		V	-1.017	-0.688	0.174	0.333	5.055
		U	0.221	-0.374	0.283	0.569	4.261
35	54	H	-0.102	-0.237	0.222	0.537	4.082
		V	-0.451	0.417	0.148	0.423	2.572
		U	0.592	0.504	0.185	0.358	3.330
36	58	H	0.044	-0.698	0.259	0.466	2.592
		V	-0.577	-0.909	0.362	0.586	2.619
		U	1.029	0.308	0.207	0.492	3.815
37	54	H	-1.076	0.426	0.259	0.500	2.912
		V	-1.665	-1.100	0.333	0.630	1.873
		U	-0.366	-0.263	0.333	0.648	1.647
38	66	H	1.328	-1.678	0.152	0.303	3.422
		V	0.924	-0.960	0.189	0.338	2.347
		U	-0.367	0.846	0.258	0.530	2.820

File no. (base*.pte)	Number of pixels	Polarisation case	Measure of centre of distribution		Measure of spread		
			Modal temperature difference	Mean temperature difference	Fraction of pixels within 0.25 K of modal temp.difference.	Fraction of pixels within 0.75 K of modal temp.difference	Standard deviation
39	87	H	5.988	2.341	0.103	0.230	3.343
		V	-0.845	1.602	0.138	0.239	3.127
		U	0.723	0.604	0.241	0.471	1.845
40	120	H	-1.809	1.488	0.133	0.225	5.350
		V	-3.488	0.790	0.083	0.205	4.636
		U	0.107	1.250	0.167	0.466	4.350
41	133	H	0.418	-2.472	0.158	0.248	4.418
		V	4.028	1.476	0.195	0.338	4.591
		U	0.056	0.812	0.150	0.363	3.806
43	553	H	4.122	4.392	0.212	0.418	3.770
		V	1.329	1.803	0.172	0.375	4.577
		U	1.810	2.241	0.174	0.421	3.545
44	715	H	-0.865	-0.578	0.359	0.692	2.752
		V	-0.984	-1.430	0.326	0.697	3.120
		U	1.695	1.753	0.203	0.449	3.597

File no. (base*.pte)	Number of pixels	Polarisation case	Measure of centre of distribution		Measure of spread		
			Modal temperature difference	Mean temperature difference	Fraction of pixels within 0.25 K of modal temp.difference.	Fraction of pixels within 0.75 K of modal temp.difference	Standard deviation
45	749	H	-1.461	-2.479	0.319	0.525	3.698
		V	3.268	0.552	0.266	0.416	4.137
		U	0.147	0.027	0.231	0.511	3.135
49	259	H	5.631	3.115	0.174	0.309	4.055
		V	4.377	1.555	0.135	0.235	3.033
		U	-0.116	0.237	0.151	0.391	3.916
50	306	H	0.910	1.558	0.225	0.458	2.831
		V	0.909	0.484	0.239	0.535	3.001
		U	2.007	1.012	0.173	0.349	2.799

V. CONCLUSIONS AND RECOMMENDATIONS

The simplified surface radiosity equation is the basis for the modeling. It states that for each pixel the radiance from the surface is the sum of the emitted radiance and reflected radiance. Since we have made the Lambertian and graybody approximations, the emitted radiance accounts for almost 95% of the radiance before atmospheric attenuation. From the comparison of apparent temperatures between the model and the images, 55% of the pixels have temperature deviations of more than 1.75K from the images. For the range of temperatures read by the thermistors, this deviation in radiance is of the order of about 3 W/m^2-sr. We can see from the SeaRad outputs (Appendix K) that the average sea and sky radiance incident on the pixel surface is of the order of 30 W/m^2-sr and 10 W/m^2-sr respectively. This gives the reflected radiance to be in the order of 1 W/m^2-sr. Therefore, the origin of the 1.75K temperature deviations for 55% of the pixels cannot to be due to the reflected radiance. A second possibility for the deviation is the path radiance due to path length error. The path radiance is of the order of 0.01 W/m^2-sr per meter increase in range. It would require a range error of more than 300m to account for the 3 W/m^2-sr deviation. Again, this is unlikely to be the source of deviations since the range or elevation error is not expected to be more than 10m. Therefore, we can conclude that the mostly likely source of the error is the surface temperature distribution used in the model. It does not sufficiently represent the actual ship skin temperature distribution.

One of the problems with modeling the temperature distribution of the ship is that there are too few thermistor readings. As a result, each plane is assumed to have a constant temperature associated with the nearest thermistor. Given the limitation on the number of thermistors, one option is to perform sensitivity analysis with the model. This will help in a better understanding of the actual temperature distribution of the ship. One approach is to perform a plane by plane analysis. Additional planes can be added to give a better distribution where necessary. Another approach may be to consider one or two

dimensional heat flow for each plane so as to arrive at a temperature distribution for the pixel surface elements.

As discussed earlier, the main contributions to the observed apparent radiance are the emitted radiance from the ship surfaces and the path radiance. Since we have assumed these two contributions to be randomly polarized, the apparent radiance that we derived from our ship model would show no significant polarization features. When our model is compared to the measured images for the three polarization cases, the match is comparable in all three polarizations. The average overall modal temperature differences are 0.078K, -0.093K and –0.093K for horizontal, vertical and random polarization respectively. The spreads of the distributions for all three polarizations are also comparable at 40-45% of the pixel within 0.75K of the mode. This shows that the assumptions used in our model are justified.

For the whole modeling process, the running of SeaRad code is the most time consuming. This is because each input file is copied to the standard input file to run the SeaRad code and the standard output file is then copied to an output file. As each pixel requires one input file, it takes approximately one hour to run a frame consisting of 360 pixels. It also takes up a lot of memory space to store the input and output files. The SeaRad input data requirement can be broken down into two types of data. The first type is the meteorological data. This data does not change for one frame and is the same for all input files of that frame. The second type is the geometry input. This is the part that changes for each pixel. If it were possible to modify the SeaRad code to accept multiple geometry input, then this would significantly reduce the processing time as well as the time spent copying files. It will make the SeaRad code a much more practical tool.

APPENDIX A. DIMENSIONS OF PLANES IN GEOMETRIC MODEL AND GENERAL DATA ON R/V POINT SUR

A. DIMENSIONS OF PLANES IN GEOMETRIC MODEL

The geometric representation of the ship is made up of 23 vertical planes. An illustration of the ship model is at Figure 2.2 in Chapter 2. The table below summarises the dimensions of each plane in the model.

Table A1. Summary Of Planes In Ship Model

Plane No.	Length (m)	Height (m)	Matched to thermistor	Description
1	12.6	4.5	10	Port hull mid section
2	6.9	4.5	4	Port hull below stack
3	7.5	2.7	2	Port hull aft section
4	9.6	3.3	8	01 deck port side
5	3.6	3.6	14	Stack port side
6	14.4	2.7	7	Starboard hull aft section
7	12.6	4.5	16	Starboard hull mid section
8	9.6	3.3	15	01 deck starboard side
9	4.8	3.3	8	02 deck portside
10	4.8	3.3	15	02 deck starboard side
11	6.9	1.8	4	Electrical switchboard room

Plane No.	Length (m)	Height (m)	Matched to thermistor	Description
				starboard side
12	3.6	3.6	12	Stack starboard side
13	9.6	2.7	2	Stern
14	4.2	1.8	4	Electrical switchboard room aft
15	5.4	1.8	7	00 deck aft
16	9.6	3.3	6	01 deck aft
17	7.2	3.3	6	02 deck aft
18	1.8	3.6	5	Stack aft
19	9.6	3.3	15	01 deck fore
20	7.2	3.3	15	02 deck fore
21	1.8	3.6	14	Stack fore
22	12.9	5.4	11	Port bow
23	12.9	5.4	16	Starboard bow

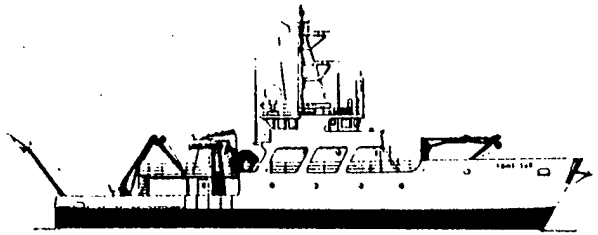

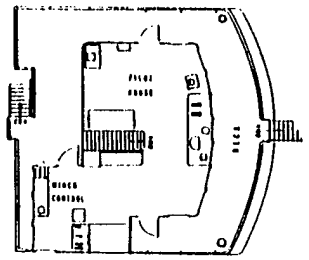

BRIDGE

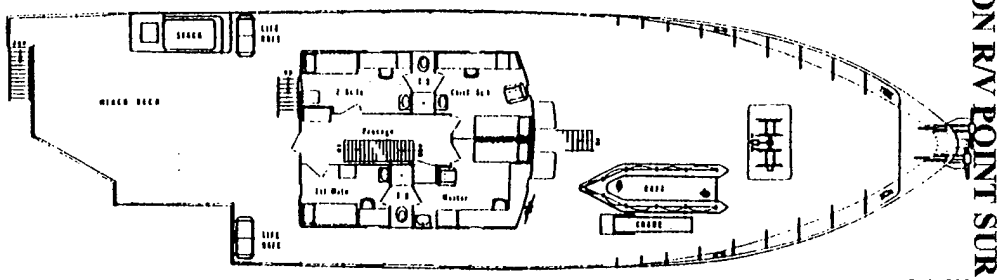

O 1 DECK

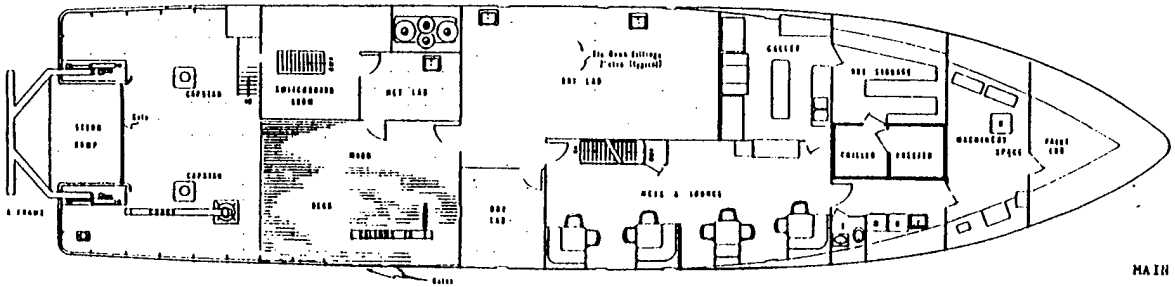

MAIN DECK

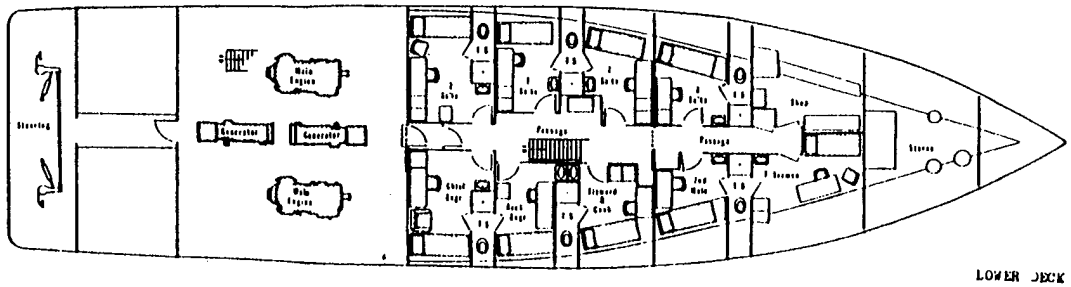

LOWER DECK

GENERAL DATA:

Length overall:	135 feet
Length between perpendiculars:	124 feet
Beam:	32 feet
Draft (full load):	9 feet
Gross tonnage:	294
Displacement (full load):	539 light tons
Maximum sustained speed:	11.5 knots
Maneuvering speed:	0-10 knots
Cruising range (normal):	5,000 nautical miles
Endurance (normal):	21 days
Weather limitations:	
Cruising sea state	#6 high (12-20 ft. waves)
Cruising Beaufort state	#8 gale (34-40 kts.)
Station sea state	#5 very rough (8-12 ft. waves)
Station Beaufort state	#7 moderate gale (28-33 kts.)
Crew:	Nine
Scientific Berthing	Twelve
Scientist (maximum)	Forty, Day Cruise only (limited by number of life jackets)
Laboratory Area:	
Dry Lab	480 sq. ft., main deck/equipment benches installed on a modular system as required, two single sinks
Electronics Lab	120 sq. ft., main deck/equipment with MK37 gyro repeater, G.P.S. readout, benches and/or electronic racks as required
Wet Lab	100 sq. ft., main deck, benches, sink installed as required
Mainmast:	Instrument platform 12 ft. long, 50 ft. above waterline
Workboat:	14 ft. Rhadial, 15 hp outboard motor
Main Deck:	1100 sq. ft., steel
Deck Handling Equipment:	Trawl Winch, Hydro Winch, CTD Winch, Fwd. Deck Crane, Aft Deck Crane, Capstain, Stern A Frame, Stbd. Gallows Frame (see section on deck handling gear for more details)
Owner:	National Science Foundation
Operator:	Moss Landing Marine Laboratories
Built:	by Atlantic Marine in 1980
Home Port:	Moss Landing, California
Radio Call Signal	WSC2276

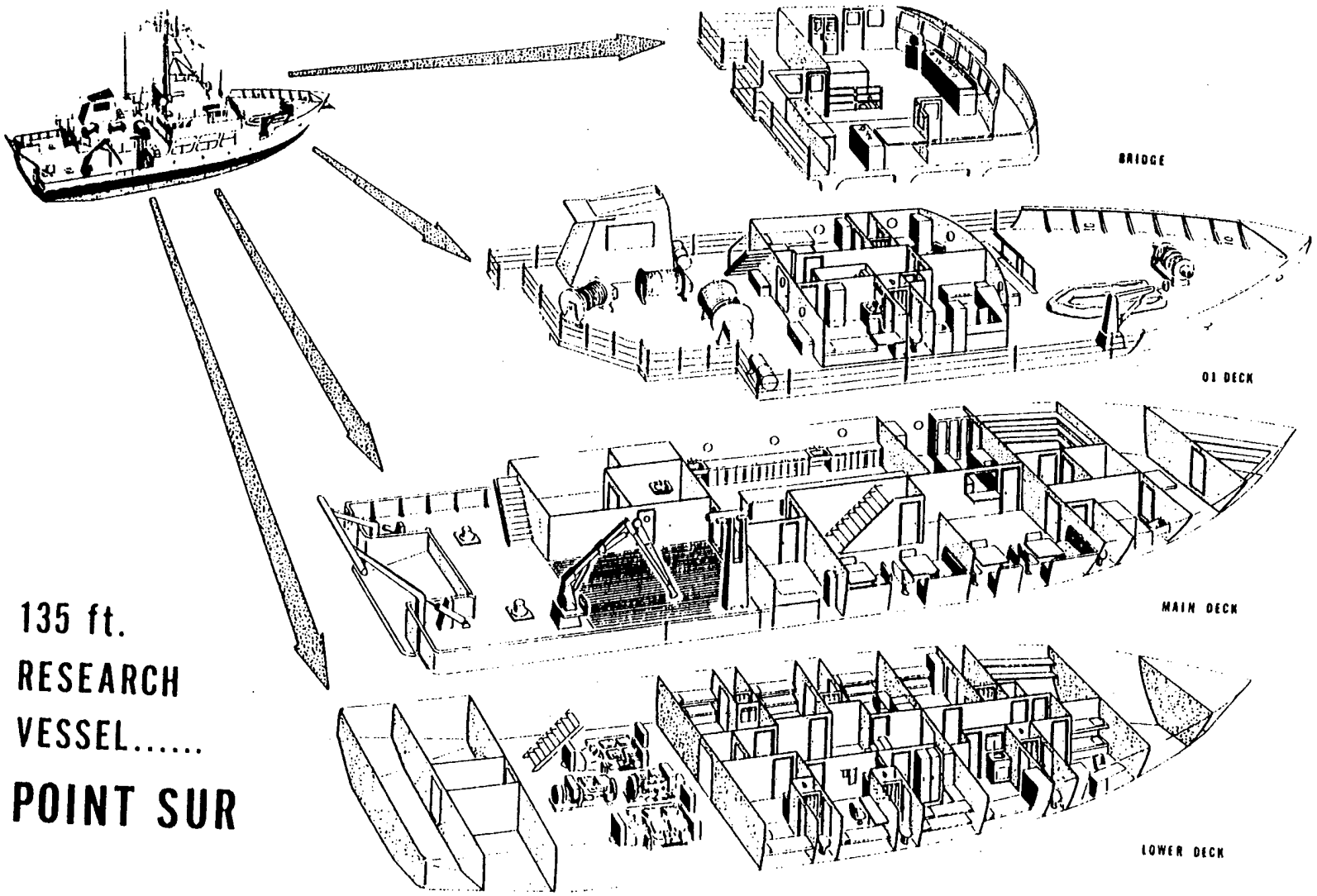

135 ft. RESEARCH VESSEL.....

POINT SUR

APPENDIX B. THERMISTOR LOCATIONS ON R/V POINT SUR

The thermistor location is described at Table B1. Figure B1 shows the locations.

Table B1. Location of thermistors

Channel No.	Location
1	Reference 25
2	Aft port
3	Aft water probe
4	Aft of stack
5	Aft on stack
6	Aft boathouse
7	Aft starboard
8	Port boathouse
9	Reference 25
10	Port below stack
11	Port bow
12	Starboard stack
13	Air
14	Port stack
15	Bow boathouse
16	Starboard bow

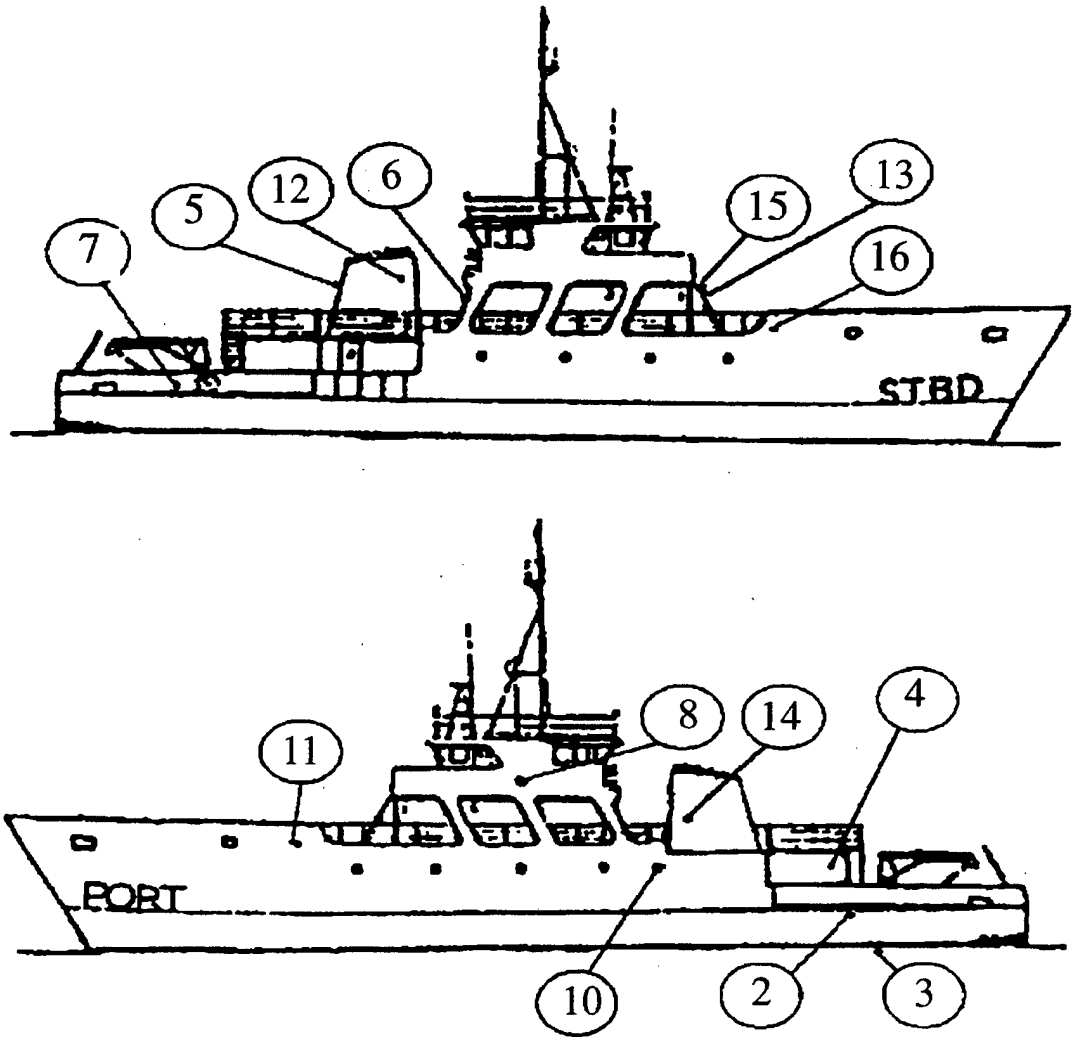

Figure B1. Location of thermistors

APPENDIX C. AVERAGE SEA AND SKY RADIANCE APPROXIMATIONS

A. AVERAGE SKY RADIANCE PATH

The sky radiance may be considered to be the sum of the sky background emission and the path radiance for a cloudless sky. It is reasonable to assume that the sky background is isotropic and therefore, sky background emission is independent of look angle. However, path radiance would increase with increasing zenith angle towards the horizon since the path length is longest at the horizon. Hence, the path representing the average sky radiance is the same path as that for the average path radiance.

To obtain the average path radiance, we consider the geometry of the atmospheric layer and the earth surface in Figure C1 below. SeaRad assumes an atmospheric layer of 100 km from the earth surface.

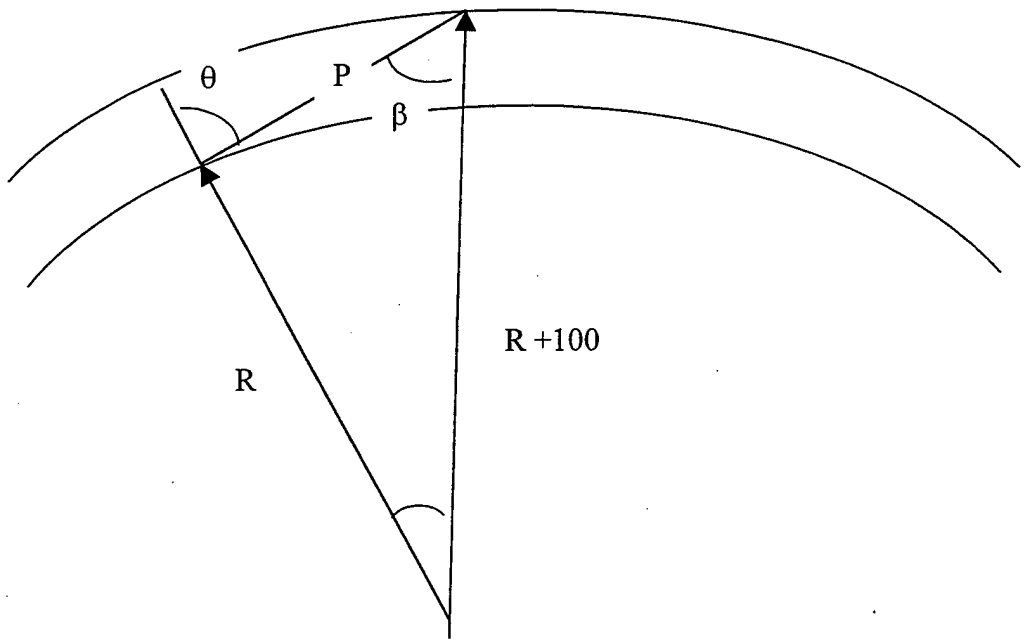

Figure C1. Relationship between zenith angle, θ and angles α and β

The angles θ, α and β are simply related by the sine rule :

$$\frac{\sin(180-\theta)}{R+100} = \frac{\sin\beta}{R} = \frac{\sin\alpha}{P} \qquad \textbf{(C.1)}$$

Therefore, we find that the path length, P is a function of θ. The average path length is then given by :

$$\langle P \rangle = \frac{2}{\pi}\int_0^{\pi/2} P(\theta)d\theta \qquad \textbf{(C.2)}$$

Performing the integral numerically, we obtain an average path length of 208 km, which corresponds to a slant path to space at a zenith angle of 65.3 degrees.

B. AVERAGE SEA RADIANCE PATH

Assuming the sea to be a flat calm surface, the sea radiance may be simplified as :

$$L_{sea} = B_{sea}(T) - \rho(\theta_i)[B_{sea}(T) - L_{sky}] \qquad \textbf{(C.3)}$$

where ρ is the reflectance given by the Fresnel equations ,

θ_i is the angle of incidence or elevation,

B_{sea} is the blackbody emission of the sea surface at temperature T and

we have assumed here that L_{sky} is the average sky radiance.

We can see that L_{sea} is also a function of the zenith angle. Since B_{sea} and L_{sky} are both constant, the path representing the average sea radiance is the same path as that for the average reflectance.

From the Fresnel equations, the E-vector amplitude reflection ratios are :

$$r_{\perp} = \frac{n_i \cos\theta_i - n_t \cos\theta_t}{n_i \cos\theta_i + n_t \cos\theta_t} \qquad \textbf{(C.4a)}$$

$$r_{//} = \frac{n_t \cos\theta_i - n_i \cos\theta_t}{n_i \cos\theta_t + n_t \cos\theta_i} \qquad \textbf{(C.4b)}$$

Taking $n_i = 1$ and $n_t = 1.33$ and making use of the Snell's law, we can find the reflectance, ρ as a function of θ_i , where :

$$\rho(\theta_i) = r_{\perp}^2 + r_{//}^2 \qquad \textbf{(C.5)}$$

Hence, the average reflectance is :

$$\langle \rho \rangle = \frac{2}{\pi} \int_0^{\pi/2} \rho(\theta_i) d\theta_i \qquad \textbf{(C.6)}$$

Again, performing the integral numerically, we found the average reflectance of the water surface to be 0.208. This value corresponds to the slant path to sea with a zenith angle of 118.1 degree.

APPENDIX D. LIST OF PROGRAMS

File Name	Type	Function
Part 1		
Start.pro	procedure	Main procedure to extract meteorological data and determine aspect angle and pixel size
Readtime	function	Reads the local time (PST) from *.pte files
Readmet.pro	function	Reads meteorological data and returns a met vector containing all the required information
Leia_pte.pro	function	Extracts the images, information or time vector
Planes.pro	function	Selects the planes that are visible for a given aspect angle
Planein.pro	procedure	Calculates the geometry inputs for SeaRad files for each pixels
Seain.pro	procedure	Writes SeaRad input files between two altitude
Avein.pro	procedure	Writes SeaRad input files for average sea and sky paths
Posn.pro	function	Calculates the position of each node
Rposn.pro	function	Calculate the position of each node after rotation to a given aspect angle
Vector.pro	function	Calculates the vector, V, from the sensor to the node position
Vsea.pro	function	Calculates the vector from the nodes to the sea
Vmag.pro	function	Calculates the magnitude of the V vector
Zenith.pro	function	Calculates the zenith angle at the sensor for each node
Part2		
Sea1	DOS batch file	Copy all input files in Case1/Inputs directory to tape 5 and call X1
X1	DOS batch file	Execute SeaRad and copy output file to Case1/Outputs directory

File Name	Type	Function
Part 3		
Continue.pro	procedure	Main procedure to continue the analysis after running SeaRad
Readtemp.pro	function	Reads the temperature matrix
Seaout.pro	function	Reads the output files from SeaRad and returns a matrix with the transmittance and path radiance
Aveout.pro	function	Reads the output files from SeaRad and returns a vector of average sky and sea radiance
Emission.pro	function	Calculates the in-band radiance
Place.pro	function	Aligns all the radiance values of planes into one matrix
Block.pro	procedure	Determines areas of overlap between planes
Overlap.pro	function	Corrects the radiance values in the overlapped area
Radtot.pro	function	Calculates the equivalent blackbody temperature from radiance
Convtemp.pro	function	Converts radiance matrix to temperature
Ttotl.pro	function	Calculates thermal level from temperature based on calibration constants
Dltotl.pro	function	Converts digital level to thermal level

APPENDIX E. STRUCTURE OF CONVERTED DATA FILE

The converted files have the following properties :

- all polarisation cases for one test case are combined into one file rather than having two separate files
-each image is a 125 x 256 integer array
- all essential information is put into a single integer matrix

The structure of the file and the format for header information is tabulated below.

Table E1. Structure Of A Basic (.Pte) File

Variable	Type
Name of the original (.PTW) file containing horizontal and vertical polarisation cases	string(20)
Information vector	integer (1,13)
Frame time : horizontal polarisation	integer (4, # frames hor.case)
Frame time : vertical polarisation	integer (4,# frames ver.case)
Frame time : unpolarised polarisation	integer (4,# frames unpol.case)
Image set (frames) : horizontal polarisation	integer (125,256,# frames hor.case)
Image set (frames) : vertical polarisation	integer (125,256,# frames ver.case)
Image set (frames) : unpolarised polarisation	integer (125,256,# frames unpol.case)

Table E2. Information Vector

Line	Data	Example
0	Day	9
1	Month	4
2	Year	96
3	Hour (first frame)	12

Line	Data	Example
4	Minute (first frame)	45
5	Seconds (first frame)	27
6	Hundreds (first frame)	77
7	Number of polarisation cases	3
8	Number of pixels per line	125
9	Number of lines	256
10	Number of frames : horizontal polarisation	27
11	Number of frames : horizontal polarisation	25
12	Number of frames : horizontal polarisation	29

APPENDIX F. LOCATION OF MEASUREMENTS

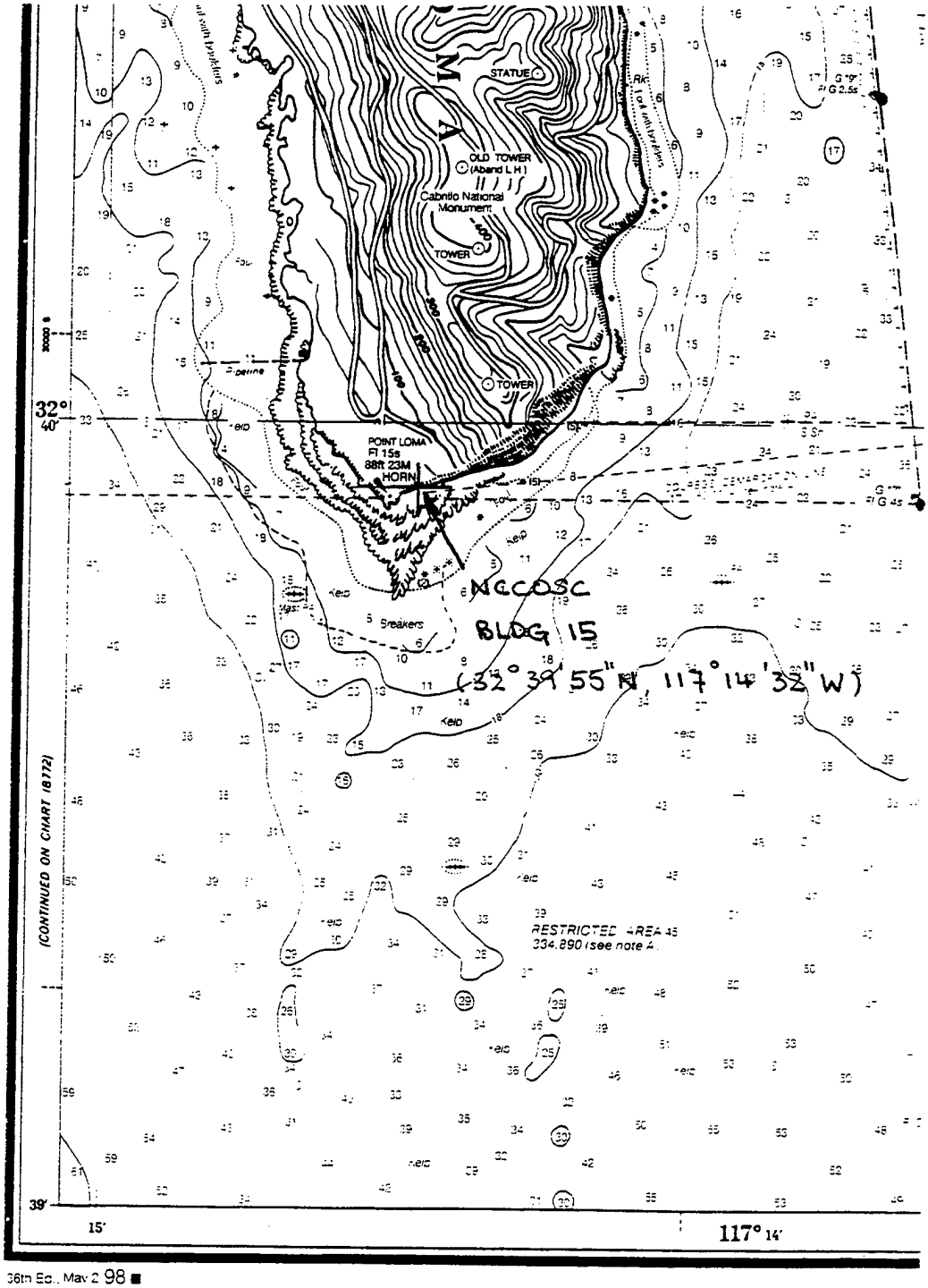

36th Ed., May 2 98 ■

18772

APPENDIX G. STORAGE FORMAT FOR METOC DATA

There were two meteorological towers installed onboard R/V Point Sur for recording the meteorological data. The storage format for the two towers are slightly different as the METOC 2 system has two additional temperature and relative humidity sensors. The two formats shall be described below.

A. METOC 1 DATA

These data files are identified by the filename "eop*.txt" where * is the GMT day of the year. Each file is started at 00:00 GMT and the data are averaged every 30 seconds and recorded. For each line of a record, the various readings from the sensors are separated by spaces across a line of text. At the end of the record, a carriage return and line feed character starts the next record on a new line. The order of the sensor readings is as follows :

01 number of readings in this average, nn
02 year, yy
03 Julian date, ddd
04 hours &minutes, hhmm
05 seconds, ss
06 relative wind speed (m/s), mmm
07 relative wind direction (degrees), ddd
08 ship speed (knots), kk.k - information not available
09 ship direction (degrees), ddd.d - information not available
10 true wind speed (m/s), mmm
11 true wind direction (degrees), ddd
12 Air temperature (degrees C), tt.t
13 relative humidity (%), pp
14 pressure (millibars), pppp.p

15 sea surface temperature (degrees C), tt.t

16 GPS time (GMT), hhmmss

17 GPS latitude (degrees & minutes), ddmm.m

18 GPS north/south indicator, either 'N' or 'S'

19 GPS longitude (degrees & minutes), , ddmm.m

20 GPS east/west indicator, either 'E' or 'W'

21 GPS speed over ground (knots), kk.k - information not available

22 GPS course over ground (degrees), ddd.d - information not available

23 GPS antenna height (m), mm.m

A sample of the data is below :

30 1996 99 2352 32 2 138 0 090 5 288 16.5 75 1016.9
16.8 000035 3311.2 N 11728.2 W 6.3 124.3 46.3

B. METOC 2 DATA

METOC 2 data files are identified by the filename "eop30sec.* " where * is the GMT day of the year. The recording format is the same as METOC 1 files except that there are 4 additional sensor readings :

01 number of readings in this average, nn

02 year, yy

03 Julian date, ddd

04 hours &minutes, hhmm

05 seconds, ss

06 relative wind speed (m/s), mmm

07 relative wind direction (degrees), ddd

08 ship speed (knots), kk.k - information not available

09 ship direction (degrees), ddd.d - information not available

10 true wind speed (m/s), mmm

11 true wind direction (degrees), ddd

12 Air temperature (degrees C), tt.t

13 relative humidity (%), pp

14 pressure (millibars), pppp.p

15 sea surface temperature (degrees C), tt.t

16 Air temperature A (degrees C), tt.t

17 relative humidity A (%), pp

18 Air temperature B (degrees C), tt.t

19 relative humidity B (%), pp

20 "***", Campbell-GPS data delimiter

21 GPS time (GMT), hhmmss

22 GPS latitude (degrees & minutes), ddmm.m

23 GPS north/south indicator, either 'N' or 'S'

24 GPS longitude (degrees & minutes), , ddmm.m

25 GPS east/west indicator, either 'E' or 'W'

26 GPS speed over ground (knots), kk.k - information not available

27 GPS course over ground (degrees), ddd.d - information not available

28 GPS antenna height (m), mm.m

A sample is below :

```
30   1996    99   2352    32     2    138     0    090     5    288   16.5    75 1016.9
16.8    0.0    0.0    0.0    0.0 *** 000035 3311.2 N       11728.2 W    6.3   124.3
46.3
```

APPENDIX H. EXTRACTED INFORMATION OF ANALYSED FILES

File no. (base*.pte)	Day of year	GMT (hrs)	Aspect angle (deg)	Range (km)	Sea temp. (^{o}C)	AMP	Current wind speed (m/s)	Average wind speed (m/s)	Wind azimuth relative to LOS (deg)	Line of Sight (LOS) (deg)
01	100	20.23	57.2	1.31	16.80	3	7.00	5.2	37.8	246.2
02	100	20.31	80.2	1.31	16.80	3	7.00	5.20	37.8	246.2
03	100	20.40	163.2	1.31	17.20	3	5.00	5.20	32.8	246.2
04	100	20.69	29.7	2.07	15.87	3	6.00	5.20	49.8	241.9
05	100	20.74	56.3	2.07	14.80	5	6.00	5.20	63.1	241.9
06	100	20.79	71.5	2.07	14.80	5	6.00	5.20	63.1	241.9
07	100	20.86	164.8	2.07	15.07	5	5.67	5.20	49.2	243.2
08	100	21.07	9.9	2.63	15.10	5	7.00	5.20	57.0	245.0
09	100	21.13	32.9	2.63	15.10	5	7.00	5.20	57.0	245.0
10	100	21.18	54.9	2.63	14.80	5	7.00	5.20	51.0	245.0
11	100	21.25	89.1	2.62	14.20	5	7.00	5.20	36.1	247.9
12	100	21.33	170.0	2.98	14.20	5	7.00	5.20	27.6	256.4
13	100	21.47	10.9	3.56	15.30	6	5.00	5.20	26.1	247.9
14	100	21.52	31.9	3.56	15.30	6	5.00	5.20	26.1	247.9

File no. (base*.pte)	Day of year	GMT (hrs)	Aspect angle (deg)	Range (km)	Sea temp. (^{0}C)	AMP	Current wind speed (m/s)	Average wind speed (m/s)	Wind azimuth relative to LOS (deg)	Line of Sight (LOS) (deg)
15	100	21.58	50.9	3.56	15.40	6	7.00	5.20	51.1	247.9
16	100	21.63	71.9	3.56	15.40	6	7.00	5.20	51.1	247.9
17	100	21.68	162.1	3.56	15.40	6	7.00	5.20	51.1	247.9
27	100	23.08	345.4	3.57	14.50	2	5.00	5.20	165.8	116.2
28	100	23.12	332.5	3.38	14.70	2	6.00	5.20	181.4	116.2
29	100	23.17	293.9	3.44	14.70	2	6.00	5.20	182.7	115.3
30	100	23.31	170.3	3.79	15.40	2	5.00	5.20	178.6	106.4
31	100	23.75	337.9	2.14	15.10	2	6.00	5.20	169.0	135.0
32	100	23.85	331.9	2.14	14.10	2	6.00	5.20	171.0	135.0
33	100	23.90	16.7	2.14	14.10	2	6.00	5.20	171.0	135.0
34	100	23.96	33.9	2.14	14.23	2	6.00	5.20	180.3	135.0
35	101	0.02	59.9	2.14	14.30	2	6.00	3.75	185.0	135.0
36	101	0.07	114.2	1.97	14.30	2	6.00	3.75	181.4	138.6
37	101	0.35	341.1	1.54	13.70	2	5.00	3.75	150.8	131.2
38	101	0.39	19.1	1.54	13.70	2	5.00	3.75	150.8	131.2
39	101	0.44	33.1	1.54	13.90	2	5.67	3.75	159.5	131.2
40	101	0.48	54.9	1.48	14.30	2	7.00	3.75	175.6	132.4
41	101	0.52	111.0	1.38	14.30	2	7.00	3.75	169.2	138.8

File no. (base*.pte)	Day of year	GMT (hrs)	Aspect angle (deg)	Range (km)	Sea temp. (^{o}C)	AMP	Current wind speed (m/s)	Average wind speed (m/s)	Wind azimuth relative to LOS (deg)	Line of Sight (LOS) (deg)
43	101	0.86	26.7	0.60	14.00	2	7.00	3.75	137.9	143.1
44	101	0.90	49.7	0.60	14.00	2	7.00	3.75	137.9	143.1
45	101	0.93	80.0	0.60	14.00	2	7.00	3.75	137.9	143.1
49	101	1.27	127.8	0.94	13.80	1	5.00	3.75	169.2	111.8
50	101	1.52	61.1	0.93	14.70	1	6.00	3.75	206.7	101.3

APPENDIX I. NAVY AEROSOL MODEL AND AIR MASS PARAMETER

A. NAVY AEROSOL MODEL [Ref. 5]

The US Navy Aerosol Model (NAM) was developed to compute the aerosol extinction coefficients for visual and infrared wavelengths over a marine boundary environment. It is built from meteorological and aerosol size spectra databases obtained near the surface layer of several oceanic environments.

The aerosol size distribution of the NAM is attributed to 3 distinct aerosol production mechanisms. The first mechanism is air mass driven while the second and third mechanisms are wind driven. Correspondingly, the NAM aerosol size distribution is a sum of 3 independent log-normal distribution functions. This is given as follows :

$$n(r) = \frac{dN}{dr} = \sum_{i=1}^{3} \frac{k}{f} A_i \exp\left[-\left(\ln\left\{ \frac{r}{fr_i} \right\} \right)^2 \right] \qquad \text{(I.1)}$$

where n(r) is the number of particles per cm^3 per radius r, in microns (μm),

k is the visibility scaling factor,

r_i are the modal radii (0.03μm, 0.24 μm and 2.0μm) measured at 80% RH, and

$A_1 = 2000\, P^2$, where P is the air mass parameter,

$A_2 = 5.866(V_{ave} - 2.2)$, where V_{ave} is the 24-hour average wind velocity,

$A_3 = 10^{(0.06V-2.8)}$, where V is the instantaneous wind velocity,

$f = [(2-Rh/100)/6(1-Rh/100)]^{1/3}$

B. AIR MASS PARAMETER [Ref. 5]

Of the 3 amplitudes A_1 to A_3 given above, the largest and the most difficult to

measure is the first one, that is, the air mass driven component. The air mass parameter, P is an integer ranging from 1 for clean oceanic air to 10 for polluted continental or coastal air.

There are several methods to obtain the air mass parameter. These methods range from measuring the atmospheric Radon-222 gas concentration to computing air mass trajectories to remote sensing using satellite. Each method has its advantages and disadvantages.

Traditionally, the Radon-222 gas concentration method is the most reliable. Radon-222 is an inert radioactive gas with a half-life of 3.82 days produced by the decay of Radium-236. Radium-236 is found in various quantities in the soils and rocks of the earth's crust. After formation in the ground, the radon diffuses into the atmosphere and becomes attached to aerosol particles that are transported by the prevailing wind over the ocean. Since radon is mainly produced on land, it is used as an air mass tracer to characterise the air mass history. The air mass parameter, P is then simply given by the equation :

$$P = INT\left[\frac{Rn}{4}\right] + 1 \qquad \textbf{(I.2)}$$

where INT truncates to the integer value and Rn is the atmospheric Radon-222 gas concentration in picocurries per cm^3. Strictly speaking, the concentration of the radon in different areas will not be the same. This is because it depends on the soil conditions, atmospheric conditions, radium deposit in the crust and strength of the radium source. Therefore, it is the relative change in radon gas concentration that is meaningful. Equation I.2, however, uses the absolute radon concentration. This is because the factor of 4 was established for the region at San Nicolas Island. This factor will have to be modified for other geographical regions.

APPENDIX J. SEARAD INPUT

SeaRad input requires the submission of a series of a minimum of 5 cards. The number of cards required depends on the mode of execution. There are a total of 19 cards of which 5 are the main cards and the rest are optional cards. A complete description of each card can be found in the file "Modtran10" that comes with program. However, this does not include the modifications done in SeaRad. The file "notes.txt" logs all the modifications and should be read in conjunction with the original card description. This appendix will only explain the parameters that are required in the cards needed in this thesis.

CARD 1 (line one) - Format (13I5, F8.3, F7.2)

MODEL, ITYPE, IEMSCT, IMULT, M1, M2, M3, M4, M5, M6, MDEF, IM, NOPRT, TBOUND, SALB

F - use LOWTRAN 7

MODEL - selects one of the 6 geographical model atmospheres or specifies that user-defined meteorological data are to be used

: *mid-latitude summer (2) was used*

ITYPE - indicates the type of atmospheric path

: *slant path to space (3) was used for average sea and sky radiance calculations and slant path between two altitudes (2) was used for pixel-sensor atmospheric compensation*

IEMSCT - selects the execution mode of the program

: *radiance mode with solar scattering (2) used*

IMULT - determines execution with multiple scattering

: *multiple scattering (1) was used*

Ml ,M2,M3,M4,M5,M6 - parameters to modify or supplement the altitude profiles of temperature and pressure, water vapor, ozone, CH_4, N_2O,CO

: *default was used (0)*

MDEF - use default profile for $C0_2$, 0_2, NO, $S0_2$, $N0_2$, NH_3, $HN0_3$

: *default was used(0)*

IM - additional switch for user defined atmosphere

: set to normal operation (0)

NORPT - switch to minimize printing of transmittance, radiance and atmospheric profile tables

: set to minimise (1)

TB0UND - boundary temperature in K

: set to sea temperature. Note : the sea temperature is only used if the path intercepts the earth

SALB - surface albedo of the earth at the location and average frequency of the calculation (0.0 to 1.0)

: set to 0

CARD 2 (line 2) - Format (6I5, 5F10.3)

IHAZE, ISEASN, IVULCN, ISCSTL, ICLD, IVSA, VIS, WSS, WHH, RAINRT, GNDALT

IHAZE - selects the aerosol model for extinction calculation and default meteorological range

: Navy aerosol model used (3)

ISEASN - selects the seasonal dependence of tropospheric and stratospheric profile

: set to default (0) i.e. model selected in card 1

IVULCN - selects the aerosol profile above the stratosphere to 100 km

: default stratospheric background used (0)

ICSTL - air mass character used only with Navy aerosol model (1 for open ocean to 10 for strong continental influence)

: calculated values from radon gas concentration used (see Appendix F)

ICLD - specifies cloud model and rain rates

: no clouds or rain (0) used

IVSA - determines the use of Army vertical structure algorithm for aerosols in boundary layer

: not used (0)

VIS - specifies meteorological range

: default used (0)

WSS - specifies current wind speed in m/s

: meteorological data used (see Appendix F)

WHH - 24 hour average wind speed in m/s

: meteorological data used

RAINRT - rain rate in mm/hr

: default used (0)

GNDALT - altitude of surface relative to sea level in km

: set to 0

CARD 3 (line 3) - Format (6F10.3, I5)

H1, H2, ANGLE, RANGE, BETA, RO, LEN

H1 - initial altitude in km (in radiance mode this always defines the altitude of the sensor)

: 0.017 km for pixel-sensor path and pixel height for sea and sky path

H2 - final altitude in km

: pixel height for pixel-sensor path and 0 for sea and sky path

ANGLE - zenith angle measured from H1 in degrees (between 0 to 180), 0 degrees is looking straight up

: calculated for each pixel

RANGE - path length in km

: not needed as the first parameter is sufficient to specify the geometry

BETA - earth center angle subtended by H1 and H2 in degrees

: not needed as the first parameter is sufficient to specify the geometry

RO - radius of the earth at the particular geographical location in km

: default radius of earth i.e. 6371.23 km (0) used

LEN - select normal or long path through tangent height calculations

: normal operation (0) used

PSI - azimuth of wind direction in degrees measured positive East of North from observer line of sight

: meteorological data used

Seaswitch - switch for turning sea modification on or off

: set to True (T)

CARD 3A1 (line 4) - Format (8F10.3)
(required when IEMSCT =2)

IPARM, IPH, IDAY, ISOURC

IPARM - controls the method of specifying solar/lunar geometry on CARD 3A2

: observer lat. and long. used (1)

IPH - determines the type of phase function to be used

: MIE generated database for LOWTRAN models (2) used

IDAY - day of the year in GMT

: calculated from meteorological data

ISOURC - type of extra-terrestrial source to be considered

: sun (0) selected

CARD 3A2 (line 5) - Format (8F10.3)

PARM1, PARM2, PARM3, PARM4, TIME, PSIPO, ANGLEM, G

PARM1 - observer latitude in degrees (-90 to +90; + means North)
: 32.917 degrees

PARM2 - observer longitude in degrees (0 to 360)
: 117.517 degrees

PARM3 - not used

PARM4 - not used

TIME - GMT time in decimal hours
: calculated from meteorological data

PSIPO - path azimuth in degrees East of North
: calculated from meteorological data

ANGLEM - phase angle of the moon
: not required

G - asymmetry factor for use with HENYEY-GREENSTEIN phase function
: not required

CARD 4 (line 6) - Format (3F10.3)

IV1, IV2, IDV, IFWHM, IFILTER

IV1 - initial frequency in wave number in cm^{-1}
: 830 cm^{-1} *i.e. 12 μm used*

IV2 - final wave number in cm^{-1}
: 1250 cm^{-1} *i.e. 8 μm used*

IDV - frequency increment in cm^{-1}
: 10 cm^{-1} *used*

IFWHM - frequency band at full width half maximum

: 5 cm^{-1} used

IFILTER - specifies the filter to be applied

: no filter (0) used

CARD 5 (line 7) - Format (I5)

IRPT

IRPT - determines what program will do next

: set to end program (0)

A sample file is shown below.

```
F 2   3   2   1   0   0   0   0   0   0   0   0   1 287.95  0.00
  3   0   0   5   0   0   0.000   7.000   5.200   0.000   0.000
  0.017   0.001  90.531   0.000   0.000   0.000   0 50.984   T
  1   2 100   0
 32.660 117.240   0.000   0.000  21.181 245.016   0.000   0.000
    830    1250      10       5       0
  0
```

APPENDIX K. SEARAD OUTPUT

The format of the SeaRad output files depends on the type of calculation that is done. Although all cases were executed in thermal plus solar radiance mode, their output is slightly different because of the way the path geometry was specified. A sample output of each case is below.

A. OUTPUT FOR AVERAGE SEA RADIANCE PATH

***** SEARAD, A MODIFICATION OF LOWTRAN7 *****

DATE: 02/08/1999 TIME: 15:09:32.87

THERMAL PLUS SOLAR RADIANCE MODE

MULTIPLE SCATTERING USED

MARINE AEROSOL MODEL USED

WIND SPEED = 6.00 M/SEC
WIND SPEED = 3.75 M/SEC, 24 HR AVERAGE
RELATIVE HUMIDITY = 76.11 PERCENT
AIRMASS CHARACTER = 2.0
VISIBILITY = .00 KM

SLANT PATH TO SPACE

H1 = .011 KM
HMIN = .000 KM
ANGLE= 118.1001 DEG

FREQUENCY RANGE

IV1 = 830 CM-1 (12.05 MICROMETERS)
IV2 = 1250 CM-1 (8.00 MICROMETERS)
IDV = 10 CM-1
IFWHM = 5 CM-1
IFILTER = 0

SUMMARY OF THE GEOMETRY CALCULATION

H1 = .011 KM
H2 = .000 KM
ANGLE = 118.100 DEG
RANGE = 0.023 KM
BETA = .000 DEG
PHI = 61.900 DEG
HMIN = .000 KM
BENDING = .000 DEG
LEN = 0

SEA AT 287.45 K REPLACES BLACK BODY BOUNDARY

UPWIND = -5.006 DEG EAST OF LINE OF SIGHT

SUMMARY OF OBSERVATION GEOMETRY

BETA = .00018 DEG
PATH AZIMUTH = 314.994 DEG EAST OF NORTH
WIND AZIMUTH = 309.988 DEG EAST OF NORTH

RECEIVER LATITUDE = 32.917 NORTH OF EQUATOR
RECEIVER LONGITUDE = 117.517 WEST OF GREENWICH
FOOTPRINT LATITUDE = 32.917 NORTH OF EQUATOR
FOOTPRINT LONGITUDE = 117.517 WEST OF GREENWICH
SUBSOLAR LATITUDE = 7.763 DEG NORTH OF EQUATOR
SUBSOLAR LONGITUDE = 179.866 DEG WEST OF GREENWICH

VALUES SEEN FROM FOOTPRINT

RECEIVER ZENITH ANGLE= 61.900 DEG
RECEIVER AZIMUTH = 174.994 DEG WEST OF UP WIND
SOLAR ZENITH ANGLE = 62.650 DEG
SOLAR AZIMUTH = 48.828 DEG WEST OF UP WIND
SOLAR SPECULAR TILT = 40.741 DEG (7.03 SIGMA, PROB = 1.720E-10)

ZERO RANGE UNPOLARIZED VALUES

SEA EMISSION = 29.68807 W M-2 SR-1 (AV. EMISS. .9426)
SKY REFLECTION = 1.05408 W M-2 SR-1
SUN GLINT = .00000 W M-2 SR-1

TOTAL RADIANCE = 30.74216 W M-2 SR-1
BLACK BODY TEMP.= 13.0 C

FULL RANGE UNPOLARIZED VALUES

SEA EMISSION = 29.14501 W M-2 SR-1
SKY REFLECTION = 1.03208 W M-2 SR-1
SUN GLINT = .00000 W M-2 SR-1
PATH TO FOOTPRINT = .64978 W M-2 SR-1 (AV. TRANS. .9792)

TOTAL RADIANCE = 30.82687 W M-2 SR-1
BLACK BODY TEMP. = 13.2 C

	HORIZONTAL (W M-2 SR-1)	VERTICAL (W M-2 SR-1)	(H-V)/(H+V) (%)
ZERO RANGE POLARIZED VALUES			
SEA EMISSION	14.26001	15.42806	-3.9
SKY REFLECTION	.85931	.17277	66.5
SUN GLINT	.00000	.00000	.0
TOTAL RADIANCE	15.13789	15.60427	-1.5
BLACK BODY TEMP. (C)	-22.0	-20.7	
FULL RANGE POLARIZED VALUES			
SEA EMISSION	14.00002	15.14499	-3.9
SKY REFLECTION	3.10762	2.22232	16.6
SUN GLINT	.00000	.00000	.0
PATH TO FOOTPRINT	.32489	.32489	.0
TOTAL RADIANCE	15.18422	15.64265	-1.5
BLACK BODY TEMP. (C)	-21.9	-20.6	

B. OUTPUT FOR PIXEL TO SENSOR PATH

***** SEARAD, A MODIFICATION OF LOWTRAN7 *****

DATE: 02/08/1999 TIME: 15:09:10.40

THERMAL PLUS SOLAR RADIANCE MODE

MULTIPLE SCATTERING USED

MARINE AEROSOL MODEL USED

WIND SPEED = 6.00 M/SEC
WIND SPEED = 3.75 M/SEC, 24 HR AVERAGE
RELATIVE HUMIDITY = 76.11 PERCENT
AIRMASS CHARACTER = 2.0
VISIBILITY = .00 KM

SLANT PATH, H1 TO H2

H1 = .017 KM
H2 = .011 KM
ANGLE = 90.367 DEG
RANGE = .000 KM
BETA = .000 DEG
LEN = 0

FREQUENCY RANGE

IV1 = 830 CM-1 (12.05 MICROMETERS)
IV2 = 1250 CM-1 (8.00 MICROMETERS)
IDV = 10 CM-1
IFWHM = 5 CM-1
IFILTER = 0

SUMMARY OF THE GEOMETRY CALCULATION

H1 = .017 KM
H2 = .011 KM
ANGLE = 90.363 DEG
RANGE = .948 KM
BETA = .009 DEG
PHI = 89.642 DEG
HMIN = .011 KM
BENDING = .000 DEG
LEN = 0

TBOUND SET TO .10 K FOR MARINE SKY

INTEGRATED ABSORPTION = 108.01 CM-1 FROM 830 TO 1250 CM-1

AVERAGE TRANSMITTANCE = .7428

MAXIMUM RADIANCE = 3.722E-02 W M-2 SR-1 (CM-1)-1 AT 830.0 CM-1
MINIMUM RADIANCE = 1.351E-02 W M-2 SR-1 (CM-1)-1 AT 1090.0 CM-1
BOUNDARY TEMPERATURE = .10 K
BOUNDARY EMISSIVITY = 1.000
FILTERED RADIANCE = 8.751E+00 W M-2 SR-1
BLACKBODY TEMPERATURE = -44.0 C

APPENDIX L. STORAGE FORMAT FOR SKIN TEMPERATURE DATA

The skin temperature of the ship was recorded through 14 thermistors attached to selected locations around R/V POINT SUR. The temperatures are read every 20 seconds and the original files are identified by the filename "flir13 /*Apr" where * is the day.

The starting time and day of the recording is 00:00 local time (PST) on the first day of each month. At top each file, the starting time and day of the first line of record of the file is also indicated. For each line of record, there are 17 entries separated by spaces across a line of text. At the end of the record, a carriage return and line feed character starts the next record on a new line. The first entry is the local time in seconds from the beginning of the first day of the month, and this is followed by the readings of the 16 thermistors in ascending order. Readings 1 and 9 are reference readings and should always be at 25.0. All temperatures are in degrees Celsius.

A sample of the data is below :

april9.1
Mon,Day,Year= 4 9 1996
Hour,Min,Sec= 20 8 27
Volts,istart,istop,nsam,iref 1.49939 1 16 100 1
763707 25.001 14.458 17.209 13.710 14.943 16.570 13.946
14.468 25.001 15.562 14.130 31.901 15.310 27.986 15.783
15.153

APPENDIX M. CALIBRATION CURVES FOR AGA-780 WITH POLARISER FILTERS

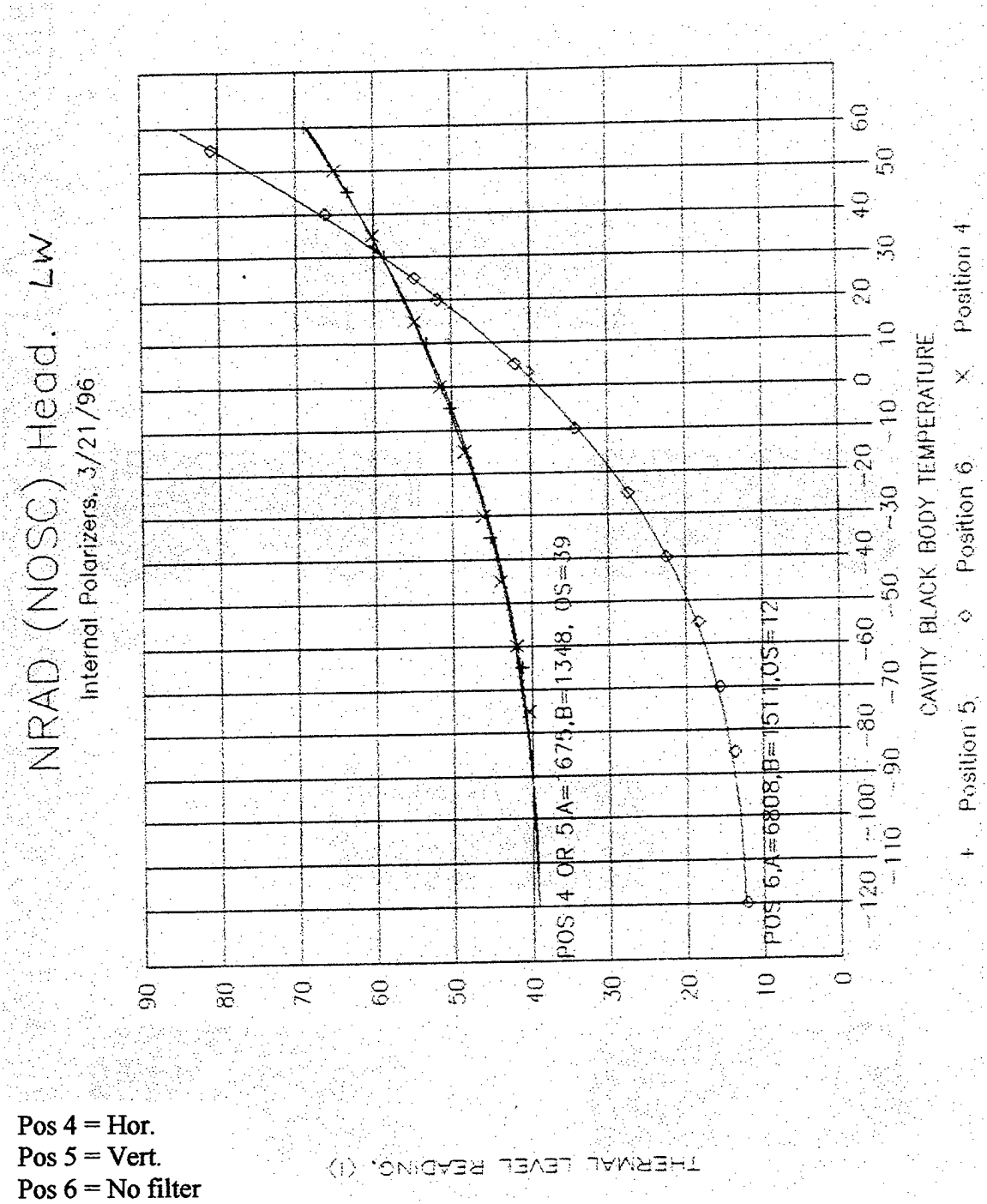

Pos 4 = Hor.
Pos 5 = Vert.
Pos 6 = No filter

APPENDIX N. ORIGINAL FILES AND R/L SETTINGS

Filename	Original filename	Range setting (R)	Level setting (L)
Base01.pte	NSCA0912.ptw	5	48
	NSCA0913.ptw	10	43
Base02.pte	NSCA0915.ptw	5	49
	NSCA0916.ptw	10	41
Base03.pte	NSCA0918.ptw	5	49
	NSCA0919.ptw	10	43
Base04.pte	NSCA0927.ptw	5	49
	NSCA0928.ptw	10	43
Base05.pte	NSCA0930.ptw	10	48
	NSCA0931.ptw	10	43
Base06.pte	NSCA0933.ptw	5	49
	NSCA0934.ptw	10	43
Base07.pte	NSCA0936.ptw	5	49
	NSCA0937.ptw	10	43
Base08.pte	NSCA0938.ptw	5	47
	NSCA0939.ptw	10	43
Base09.pte	NSCA0940.ptw	5	47
	NSCA0941.ptw	10	44
Base10.pte	NSCA0942.ptw	5	47
	NSCA0943.ptw	10	43
Base11.pte	NSCA0944.ptw	5	47
	NSCA0945.ptw	10	44
Base12.pte	NSCA0946.ptw	5	48
	NSCA0947.ptw	10	44
Base13.pte	NSCA0948.ptw	5	47
	NSCA0949.ptw	10	43

Filename	Original filename	Range setting (R)	Level setting (L)
Base14.pte	NSCA0950.ptw	5	47
	NSCA0951.ptw	10	44
Base15.pte	NSCA0952.ptw	5	46
	NSCA0953.ptw	10	43
Base16.pte	NSCA0954.ptw	5	46
	NSCA0955.ptw	10	44
Base17.pte	NSCA0956ptw	5	47
	NSCA0957.ptw	10	44
Base27.pte	NSCA0978.ptw	5	49
	NSCA0979ptw	10	43
Base28.pte	NSCA0980.ptw	10	51
	NSCA0981.ptw	10	44
Base29.pte	NSCA0982.ptw	5	51
	NSCA0983.ptw	10	45
Base30.pte	NSCA0988.ptw	5	51
	NSCA0989.ptw	10	44
Base31.pte	NSCA0990.ptw	5	47
	NSCA0991.ptw	10	43
Base32.pte	NSCA0993.ptw	5	49
	NSCA0994.ptw	10	43
Base33.pte	NSCA0996.ptw	5	49
	NSCA0997.ptw	10	43
Base34.pte	NSCA0999.ptw	5	49
	NSCA1000.ptw	10	43
Base35.pte	NSCA902.ptw	5	49
	NSCA903.ptw	10	43
Base36.pte	NSCA905.ptw	5	50
	NSCA906.ptw	10	43

Filename	Original filename	Range setting (R)	Level setting (L)
Base37.pte	NSCA911.ptw	5	50
	NSCA912.ptw	10	44
Base38.pte	NSCA914.ptw	5	50
	NSCA915.ptw	10	43
Base39.pte	NSCA917.ptw	10	51
	NSCA918.ptw	10	43
Base40.pte	NSCA920.ptw	10	51
	NSCA921.ptw	10	44
Base41.pte	NSCA923.ptw	5	50
	NSCA924.ptw	10	42
Base43.pte	NSCA929.ptw	5	49
	NSCA930.ptw	20	44
Base44.pte	NSCA932.ptw	5	49
	NSCA933.ptw	20	43
Base45.pte	NSCA935.ptw	5	49
	NSCA936.ptw	20	47
Base49.pte	NSCA947.ptw	5	49
	NSCA948.ptw	10	43
Base50.pte	NSCA958.ptw	5	51
	NSCA959.ptw	10	44

APPENDIX O. AN EXTRACT ON PERFORMING COMPLEX THERMAL MEASUREMENTS FROM THE AGA MANUAL [Ref.9]

Section 10 of the AGA operating manual describes the thermal measurement techniques for making measurements with the AGA Thermovision infrared scanner. The extract in the next three pages describes the theory and how complex thermal measurements are made with the AGA scanner.

area) is just brightened up by the isotherm. For ease of operation this is often carried out with the PICTURE MODE switch set to INVERTED or BLACK.

(c) Adjust the second isotherm (LEVEL 2) to indicate the colder of the two areas of interest. If this cannot be achieved, increase the THERMAL RANGE one step at a time and repeat (a) and (b) and (c) again until both colder and warmer areas are covered by the same selected range.

NOTE: For overall accuracy maintain the THERMAL RANGE setting at its lowest level consistent with displaying both the reference and object area isotherms.

Without readjusting THERMAL RANGE or LEVEL proceed as follows:

(d) Carefully adjust the two isotherm controls to indicate the object area to be measured and the reference area respectively. This is shown by the areas being displayed as saturated white.

(e) Read the isotherm scale values at the top edge of both isotherm markers, calculate the difference and multiply by the THERMAL RANGE setting (see figure 2).

This results in a thermal difference value $\pm i_{or}$ that can be applied directly to the calibration curve since we have postulated $\epsilon_o = \epsilon_r = 1$ and $\tau_o = 1$. Proceed as follows:

(f) Mark the reference temperature on the calibration chart. Read via the curve the corresponding thermal value i_r. Add the thermal difference value $\pm i_{or}$ obtained in (e) to I_r. This gives the blackbody thermal value I_o of the object, which is then converted to temperature t_o by means of the curve.

NOTE: If the reference should have higher temperature than the object, the thermal difference $\pm i_{or} = i_o - i_r$ becomes negative and should consequently be subtracted from the reference thermal value i_r. The lower half of the isotherm scale has negative readings. It is therefore important to note the correct sign of the isotherm scale readings when calculating $i_o - i_r$.

COMPLEX THERMAL MEASUREMENTS

The previous instructions have assumed the ideal situation, that the object is a perfect blackbody and that no external factors influence the measurements.

In complex thermal measurement situations, however, where several factors influence the measurements, the true object temperature has to be derived by calculation.

An expression is set up to include the radiation that reaches the scanner from the object. From this expression the unknown parameter is extracted (e.g. object temperature or object emissivity). Before this derivation is carried out the following variables should be considered.

Variables affecting measurement

The most important external influencing factors are:

Emissivity – Actual objects are seldom "black". The emissivity factor must therefore often be taken into account in infrared temperature measurements as detailed in the measurement formulae. Individual object emissivity can be measured or can be found in tables, (e.g. Table 1 page 11.8).

Ordinarily, object materials and surface treatments exhibit emissivities ranging from approximately 0.1 to 0.95. A highly polished (mirror) surface falls below 0.1, while an oxidised or painted surface has greatly increased emissivity. Oil-based paint, regardless of colour in the visible spectrum, has an emissivity over 0.9 in the infrared. Human skin exhibits an emissivity close to 1 which is used of in medical thermography for direct body-temperature readings.

Surroundings – The reflectivity factor of an opaque, diffuse surface is $\zeta = 1 - \epsilon$.

A low emissivity factor means therefore not only that the emission from the object is lower than from a blackbody of the same temperature. It also means that undesired radiation from the surroundings is reflected into the scanner. The measurement formulae is corrected for reflected radiation by means of a term including I_s, which is related to ambient temperature. It is therefore important that the object surroundings have a homogenous (ambient) temperature and do not include hot areas so positioned that their radiation can be reflected by the object. Sometimes an efficient ambient temperature has to be estimated to take into account radiation sources that cannot be removed or shielded.

Object opacity – Objects may be more or less transparent to infrared radiation e.g. glass and plastics. The radiation received from such an object would include irrelevant transmitted radiation from the background. Besides the efficient emissivity would be low and hard to estimate. However, the spectral characteristics of the scanner may be adapted to the object by means of spectral filtering such that only spectrum regions where the emissivity is high and the transmission is zero are utilised. Where this is possible to do, thermal measurements can be carried out. However, the resultant emissivity and reflectivity of the object must still be taken into account if the spectral filtering does not result in an effective blackbody.

Object size – The detector subtends a certain solid angle in the object space. If the object does not cover this angle the detector will receive radiation from the object background. This will tend to lower the temperature difference indicated between the object and background. It is therefore recommended that the size of the image area, where temperature is to be measured, should not be less than 2.5 x 2.5 mm as seen on the Black/White monitor chassis display screen.

The Atmosphere – Certain constituents of the atmosphere absorb infrared radiation in the spectral bands being used. The most important gases are water vapour (H_2O) and carbon dioxide (CO_2). This absorption will attenuate the infrared radiation, from the object to the instrument. In some cases (e.g. hot combustion

flames) the self-emission of atmospheric gases is very high and has to be taken into consideration.

The atmospheric attenuation can be calculated and compensated with great accuracy using either computer programs or an approximative formula. (See Section 10 page 10.6.)

Measurement formulae

In general a number of different parameters are involved in temperature determinations using radiometric methods. Here are listed all parameters used in the following description. They are divided into three groups of which the last is used only for formula derivation.

Radiation source and atmosphere related parameters

t_o = object temperature (°C)

t_a = temperature of object surroundings (ambient) (°C)

t_r = reference temperature (°C)

t_{atm} = atmosphere temperature (°C)

ϵ = emissivity factor, $0 \leq \epsilon \leq 1$ ($\epsilon = 1$ for a "blackbody")

ϵ_o = object emissivity

ϵ_r = emissivity of reference surface

ϵ_a = emissivity of object surroundings ϵ_a is considered ≈ 1

τ_o = atmospheric correction factor for the atmosphere between scanner and object, i.e. atmospheric transmission corrected for systems spectral response

τ_r = as above for the atmosphere between scanner and reference

d_o = distance scanner to object (m)

d_r = as above to reference (m)

I = calibrated thermal value. Refers to the instruments calibration function (graphical curve or calculator program) which describes the relation between object blackbody temperature and instrument numerical output on short distance. $I = f(t)$ (IU)

I_o = calibrated thermal value for $t = t_o$ (IU)

I_a = calibrated thermal value for $t = t_a$ (IU)

I_r = calibrated thermal value for $t = t_r$ (IU)

I_{atm} = calibrated thermal value for $t = t_{atm}$ (IU)

Instrument reading parameters

I_o' = measured object thermal value. Instrument reading of radiation received from the object surface via the atmosphere (IU)

I_r' = as above for the reference (IU)

The instrument reading consists of two terms: $i' = L - i$, where

L = THERMAL LEVEL setting of the instrument (IU)

L_o = as above at object measurement (IU)

L_r = as above reference measurement (IU)

i = measured relative thermal value = instrument scale or display reading x THERMAL RANGE setting (IU)

i_o = as above referring to object measurement (IU)

i_r = as above referring to reference measurement (IU)

Δi_{or} = as above referring to the difference between object and reference measurement (IU)
$\Delta i_{or} = i_o - i_r$

Radiation notations

S = received and detected radiation from a blackbody of temperature t, at short distance (Photons/sec)

S_o = as above when $t = t_o$ (Photons/sec)

S_a = as above when $t = t_a$ (Photons/sec)

S_{atm} = as above when $t = t_{atm}$ (Photons/sec)

S_o' = radiation received via the atmosphere from the object surface (Photons/sec)

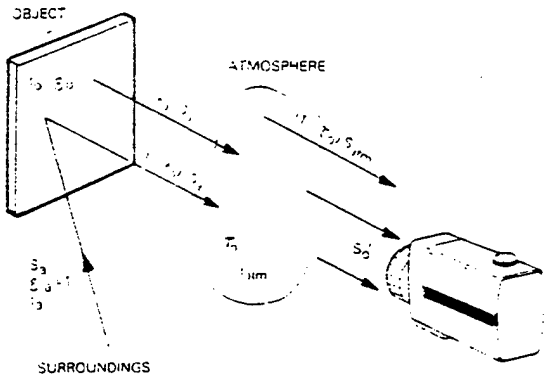

Fig. 3 Radiation conditions in the general measurement situation

Figure 3 illustrates schematically the radiation conditions in the general measurement situation. Note that the reflection factor of the object surface is $1 - \epsilon_o$ for an opaque object, and that the emission factor of the atmosphere is $(1 - \tau_o)$. With the support of this figure the received radiation can be written:

$S_o' = \tau_o \cdot \epsilon_o \cdot S_o + \tau_o (1 - \epsilon_o) S_a + (1 - \tau_o) S_{atm}$
= object radiation + reflected radiation − atmosphere radiation

This radiation relationship can be converted into a thermal value relationship by utilising the fact that AGA Thermovision® 780 has a linear, photon counting detector.

We can therefore write the thermal value

$$I = C \times S$$

where C is an empirical instrument factor

Replacing S_o', S_o, S_a and S_{atm} by $\frac{I_o'}{C}$, $\frac{I_o}{C}$, $\frac{I_a}{C}$ and $\frac{I_{atm}}{C}$ respectively results in

$$I_o' = \tau_o \epsilon_o I_o + \tau_o (1-\epsilon_o) I_a + (1-\tau_o) I_{atm} \quad (1)$$

This is the general measurement formula describing how the measured thermal value I_o' relates to the three radiation sources: object, surroundings and atmosphere, together with their associated parameters emissivity and transmission. The object is considered opaque (i.e. no transmitted radiation through the object) and all the relevant surrounding surfaces are assumed to have the same (ambient) temperature t_a (from that assumption follows automatically $\epsilon_a = 1$)

The radiation terms are expressed as blackbody thermal values determined by the calibration function at respective source temperature.

This formula is a suitable starting point for derivation of special measurement formulae adapted to special measurement situations.

For **direct measurements** (without reference) the formula can be rewritten, using the relation $I_o' = L_o - i_o$. Solve for I_o:

$$I_o = \frac{L_o - i_o}{\tau_o \epsilon_o} - \left(\frac{1}{\epsilon_o} - 1\right) I_a - \frac{1}{\epsilon_o}\left(\frac{1}{\tau_o} - 1\right) I_{atm} \quad (2)$$

In case the object temperature is known but the object emissivity unknown, the latter can be calculated. Solve for ϵ_o:

$$\epsilon_o = \frac{L_o + i_o - \tau_o I_a - (1-\tau_o) I_{atm}}{\tau_o (I_o - I_a)} \quad (3)$$

For **relative measurements** with a known temperature reference, corresponding formulae are derived as follows:

$$I_o' = \tau_o \epsilon_o I_o + \tau_o (1-\epsilon_o) I_{ao} + (1-\tau_o) I_{atm}$$

$$I_r' = \tau_r \epsilon_r I_r + \tau_r (1-\epsilon_r) I_{ar} + (1-\tau_r) I_{atm}$$

where I_{ao} and I_{ar} refer to the surroundings of object and reference respectively.

$$I_o' - I_r' = L_o - i_o - L_r - i_r = L_o - L_r - \Delta i_{or}$$

As previously described under relative measurements, the THERMAL LEVEL should be kept constant when using this method. Thus $L_o = L_r$ and from that follows:

$$I_o' - I_r' = \Delta i_{or}$$

in a practical measurement situation, we assume that object and reference are placed close together. Hence $\tau_r = \tau_o$ and $I_{ao} = I_{ar} = I_a$. With these assumptions we get

$$I_o = \frac{\Delta i_{or}}{\tau_o \epsilon_o} + \frac{\epsilon_r}{\epsilon_o} I_r + \left(1 - \frac{\epsilon_r}{\epsilon_o}\right) I_a \quad (4)$$

Solve for ϵ_o:

$$\epsilon_o = \frac{\Delta i_{or} + \tau_o \epsilon_r (I_r - I_a)}{\tau_o (I_o - I_a)} \quad (5)$$

The above derivated formulae can be a great deal simplified under special conditions. For instance if all ϵ and τ are close to unity we get

$$I_o \approx I_o' \text{ and } I_o \approx \Delta i_{or} + I_r$$

for direct and relative measurement respectively, i.e. as assumed in the first part of this section.

The formula for relative measurement will be reduced and thereby the overall accuracy improved, if $\epsilon_o = \epsilon_r$ and $\tau_o = \tau_r$.

This requirement is met if for example the reference surface is a part of the object surface itself where the temperature is known. The formula is then reduced to

$$I_o = \frac{\Delta i_{or}}{\tau_o \epsilon_o} + I_r$$

ATMOSPHERIC INFLUENCE ON INFRARED TEMPERATURE MEASUREMENTS

The atmosphere is not fully transparent to infrared radiation. It attenuates radiation passing through it and also emits radiation, the amount dependent on the temperature.

The measurement formulas previously described indicated how to correct for the atmospheric influence provided that the correction factor τ is known. τ depends on a number of parameters. The most important parameters are listed below together with the actual values for what is defined as "standard atmosphere". (See Table 1.)

Table 1 Parameters influencing the atmospheric correction factor τ

Parameter	Standard atmosphere
Scanner type (SW, 8BAR, LW)	
Distance scanner to object	
Air temperature	15°C
Air pressure	1 atm = 1013 mb
Relative humidity (H_2O)	50%
Carbon dioxide (CO_2)	300 ppm
Carbon monoxide (CO)	1 ppm
Dinitrogen oxide (N_2O)	0.3 ppm
Ozone (O_3)	0.355 ppm
Methane (CH_4)	2 ppm
Aerosol visibility (particles)	10 km

LIST OF REFERENCES

1. Cooper A.W., Lentz W.J., Walker P.L., Chan P.M., *"Polarization Enhancement of Contrast in Infrared Ship/Background Imaging"*, Paper 26, AGARD SPP Symposium on Propagation Assessment in Coastal Environments 1994, AGARD Proceedings CP576, pp.26.1-26.10, 1995 .

2. Moretz D.G., *"Analysis of target contrast improvement using polarisation filtering in the infrared region"*, Master's Thesis, Naval Postgraduate School, Dec 1994.

3. Zeisse, C.R., *"SeaRad, A Sea Radiance Prediction Code"*, Technical report 1702, Naval Command, Control and Ocean Surveillance Centre, RDT and E Division, Nov 1995.

4. C.Cox and W.Munk, *"Measurement of the roughness of the sea surface from photographs of the sun's glitter"*, Journal of Optical Society of America, Vol 44, No.11, Nov 1954.

5. Niple E.R., *"General scattered light (GSL) model for advanced radiance calculations"*, Aerodyne Research Inc., Proceedings of SPIE, Vol 2469, pp.197, 1995.

6. Johnson K.R. and Rodriguez L.J., *"User's manual for Thermal Contrast Model 2 (TCM2)"*, Georgia Tech Research Institute, Oct 1990.

7. Pontes M.C., *"Polarisation effects on infrared target contrast"*, Master's Thesis, Naval Postgraduate School, Aug 1998.

8. Battalino T.E.,*"Air mass characterisation for optical propagation modeling in the coastal marine atmosphere"*, Naval Air Warfare Centre Weapons Division, Proceedings of SPIE, vol 3125, pp.47,1997.

9. AGA Thermovision 780 operating manual, AGA Infrared Systems AB, Publication No. 556 492, ed. II,1980.

10. Saunders P.M., *"Radiance of sea and sky in the infrared window 800-1200 cm^{-1} "*, Journal of Optical Society of America, vol 58, no.5, May 1968.

INITIAL DISTRIBUTION LIST

1. Defense Technical Information Cente..... 2
   8725 John J. Kingman Rd., STE 0944
   Ft. Blevoir,VA 22060-6218

2. Dudley Knox Library..... 2
   Naval Postgraduate School
   411, Dyer Rd.
   Monterey, CA 93943-5101

3. Professor A.W.Cooper,Code PH/Cr..... 2
   Department of Physics
   Naval Postgraduate School
   Monterey, CA 92943-5117

4. Professor R.J.Pieper, Code EC/Pr..... 1
   Department of Electrical and Computer Engineering
   Naval Postgraduate School
   Monterey, CA 92943-5117

5. Naval Sea Systems Command.....1
   PEO-Theater Air Defence, Ship Self Defense
   Attn : Mr J.E. Misanin, PEO-TAD D-234
   Washington, DC 20363-5100

6. Naval Space and Naval Warfare Systems Center.....1
   Propagation Division
   Attn : Dr J.H. Ritcher, Code 88
   53570 Silvergate Ave
   San Diego,CA 92152-5230

7. Naval Space and Naval Warfare Systems Center.....1
   RDT & E Division
   Attn : Dr D.R. Jensen
   53570 Silvergate Ave
   San Diego,CA 92152-5230

8. Maj. Tan Chee Yong 2
   NPLD-HQ RSN
   MINDEF Building
   303, Gombak Drive
   SINGAPORE 669645